

**Local paths to global coherence: Cutting networks down to size**Yu Hu,<sup>1</sup> James Trousdale,<sup>2</sup> Krešimir Josić,<sup>2,3,\*</sup> and Eric Shea-Brown<sup>1,4,5,\*</sup><sup>1</sup>*Department of Applied Mathematics, University of Washington, Seattle, Washington 98195, USA*<sup>2</sup>*Department of Mathematics, University of Houston, Houston, Texas 77204-5001, USA*<sup>3</sup>*Department of Biology and Biochemistry, University of Houston, Houston, Texas 77204-5001, USA*<sup>4</sup>*Program in Neurobiology and Behavior, University of Washington, Seattle, Washington 98195, USA*<sup>5</sup>*Department of Physiology and Biophysics, University of Washington, Seattle, Washington 98195, USA*

(Received 13 December 2012; revised manuscript received 11 December 2013; published 10 March 2014)

How does connectivity impact network dynamics? We address this question by linking network characteristics on two scales. On the global scale, we consider the coherence of overall network dynamics. We show that such *global coherence* in activity can often be predicted from the *local structure* of the network. To characterize local network structure, we use “motif cumulants,” a measure of the deviation of pathway counts from those expected in a minimal probabilistic network model. We extend previous results in three ways. First, we give a combinatorial formulation of motif cumulants that relates to the allied concept in probability theory. Second, we show that the link between global network dynamics and local network architecture is strongly affected by heterogeneity in network connectivity. However, we introduce a network-partitioning method that recovers a tight relationship between architecture and dynamics. Third, for a particular set of models, we generalize the underlying theory to treat dynamical coherence at arbitrary orders (i.e., triplet correlations and beyond). We show that at any order, only a highly restricted set of motifs impacts dynamical correlations.

DOI: [10.1103/PhysRevE.89.032802](https://doi.org/10.1103/PhysRevE.89.032802)

PACS number(s): 89.75.Hc, 87.19.lj, 02.70.-c, 05.40.-a

**I. INTRODUCTION**

From genetics to neuroscience to the social world, networks of stochastic dynamical systems are ubiquitous. The architecture of these networks is complex: irregular but far from random, with an unexpected prevalence of specific connection features [1–5]. At the same time, networks produce complex patterns of collective dynamics [6–8]. Here we explore the links between these two phenomena and provide general principles that relate network architecture to collective dynamics.

The joint activity of pairs and groups of nodes is frequently described using pairwise [9] and higher-order correlations (coherence) [10–14]. But what do such measures of coherence tell us? A high average correlation (across all node pairs) reflects approximate synchrony. In some settings, this global synchrony is what matters for how strongly a network will “cooperate” to influence a system downstream [15–19]. Beyond the impact on downstream targets, synchrony can also have an impact on how information is encoded in network activity. This has been widely studied in the neural networks of sensory pathways, which encode signals from the external world; here, synchronous fluctuations can either serve as a separate “channel” or can modulate the amount of information that network responses can carry by shaping their overall signal-to-noise ratiocinates [20–25].

We thus turn to the question of relating coherent network dynamics to connectivity structure as described by a directed graph specifying node interactions. Despite significant progress [10–12,26,27], this problem remains a challenge. One approach is to identify the key *local* connectivity features of a complex network that predict *global* levels of correlation—the

averaged correlation across all nodes in the network. The local connectivity is characterized using specific pathways between subsets of nodes, or motifs. Formally, motifs are particular connectivity patterns (usually smaller graphs) that occur, possibly multiple times, in the graph of the network. Several example network motifs are shown in Fig. 1.

How can motif structure be used to predict networkwide correlation? An approximate expression relating correlations to the frequency of different types of network motifs has been derived previously [11,28]. Although this result led to a number of insights, it is difficult to apply generally due to the combinatorial explosion of motifs that appears in the approximation [11,28,29]. It is necessary to measure empirically the frequencies of many different motifs in order to apply the theory. In earlier work, we sought to simplify the situation [29]. We used the frequency of a few, smaller motifs to predict the frequency of larger motifs in the network. As a result, we showed that the frequency of a few small motifs alone could predict networkwide correlation—in many cases with a high level of accuracy.

However, three key questions remain unanswered. First, under what conditions can a set of small motifs be used to accurately infer the frequency of large motifs? Second, what features of network connectivity, or motifs, predict higher-order correlations? Third, when our earlier methods fail [29]—that is, when the frequency of small motifs alone does not provide accurate information about correlations—is there a way to still cut the dynamical complexity down to size?

In this paper, we answer these questions. We first summarize and, where necessary, reinterpret our earlier results [29] employing combinatorial definitions: Borrowing ideas from probability theory, we define motif moments and cumulants. This abstract approach both reveals the probabilistic structure of our underlying assumptions and allows us to immediately generalize our theory to link higher-order correlations in

\*These authors contributed equally.

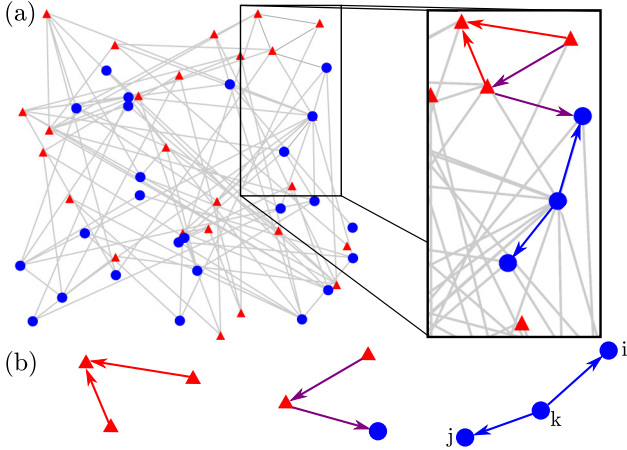


FIG. 1. (Color online) (a) We consider directed, recurrent networks within which motifs of different orders, i.e., number of edges, are identified. The inset illustrates how these motifs are embedded in the graph. The different shape and color of nodes become relevant and are explained in Sec. IV A. (b) Left to right: second-order converging, chain, and diverging motifs, as highlighted with color in the inset of (a). Only the latter two contribute to correlations in the path expansion given by Eq. (4).

network dynamics to graphical features described by frequencies of more complex motifs. Intriguingly, only a highly restricted set of motifs enters in expressions for dynamical correlations of any given order. We explicitly identify these motifs associated with every order. Finally, we apply our method to various types of networks, and show that heterogeneity in network connectivity can lead to a failure of the predictive approach in [29]. However, even in this case, an accurate approximation can be obtained if the network is correctly partitioned and motif frequencies are measured within and across the partitions.

Our results for coherence at both second and higher orders hold for stochastic networks where node interactions can be described using linear response, including linear stochastic differential equations (Ornstein-Uhlenbeck) and shot noise processes [30] on networks. Moreover, our findings for second- (but not higher-) order coherence also hold for coupled point process systems, including networks of integrate-and-fire neurons [28] as well as linearly interacting point processes (Hawkes models [11,31]).

## II. STOCHASTIC DYNAMICS ON NETWORKS

### A. Model of stochastic dynamics on networks

Stochastic networks of  $N$  linearly interacting units can generally be described using

$$y_i(t) = x_i(t) + A_i(t) * \sum_j \mathbf{W}_{ij} y_j(t). \quad (1)$$

Here the activity of the  $i$ th node,  $y_i(t)$ , is perturbed linearly from a (stochastic) baseline  $x_i(t)$  by filtered input ( $*$  stands for convolution) from the rest of the network. The response of unit  $i$  is captured by its linear response function  $A_i(t)$ , and  $\mathbf{W}_{ij}$  is the connection strength of the input from unit  $j$  to unit  $i$ . An example of such a stochastic system includes the multivariate

Ornstein-Uhlenbeck (OU) process, widely used to model biological networks [32–35]. We illustrate many of our ideas using this OU process. Details about how the OU process can be put into the form of Eq. (1) are in the Appendix, Sec. 1, and details about our numerical results are in the Appendix, Sec. 3.

For simplicity, we assume that connection weights are uniform and equal to  $w$ , so that  $\mathbf{W} = w\mathbf{W}^0$  for an adjacency matrix  $\mathbf{W}^0$ . We also assume that the nodes are homogeneous in their dynamics and response to inputs, so that  $A_i(t) = A(t)$ , and  $x_i(t)$  are independent and identically distributed processes. These assumptions can be relaxed, as explained in [29].

### B. Cross correlation and network motifs

Our goal is to relate network architecture, described by the matrix  $\mathbf{W}$ , to coherence in network dynamics. At second order, coherence is measured by the cross covariance between the activities of nodes  $i$  and  $j$  as a function of time lag  $\tau$ ,  $(C_y(\tau))_{ij}$  [9]. As computations are simpler in the spectral domain, we first consider the cross spectra,  $S_y(\omega) = \mathbf{E}[\bar{y}\tilde{y}^T]$  [36], of the processes  $[\tilde{x}(\omega) = \mathcal{F}(x(t))]$  represents the Fourier transform,  $\bar{z}$  is a complex conjugate,  $T$  denotes a transpose, and bold symbols represent column vectors or matrices]. Cross spectra and cross covariances are related by the Wiener-Khinchin theorem,  $S_y(\omega) = \mathcal{F}(C_y(\tau))$  [37].

After a Fourier transformation, the matrix form of Eq. (1) is

$$\tilde{y}(\omega) = \tilde{x}(\omega) + \tilde{A}(\omega)\mathbf{W}\tilde{y}(\omega). \quad (2)$$

Here,  $\mathbf{y}$  and  $\mathbf{x}$  are column vectors of collections of  $y_i$  and  $x_i$ , respectively. If the spectral radius of  $\tilde{A}(\omega)\mathbf{W}$  [denoted by  $\Psi(\tilde{A}(\omega)\mathbf{W})$ ; same below] is less than 1, then Eq. (2) implies  $\tilde{y} = (\mathbf{I} - \tilde{A}\mathbf{W})^{-1}\tilde{x}$ , where  $\mathbf{I}$  is the identity matrix. This leads to the following relation between the matrix of cross spectra and autospectra of the isolated (baseline) nodes:

$$S_y(\omega) = (\mathbf{I} - \tilde{A}\mathbf{W})^{-1}S_x(\omega)(\mathbf{I} - \tilde{A}\mathbf{W}^T)^{-1}. \quad (3)$$

This shows how the baseline variability within individual nodes,  $S_x(\omega) = S_x(\omega)\mathbf{I}$ , propagates through the network. An analog of Eq. (3) holds for networks of integrate-and-fire neurons and Hawkes processes [28,31].

Equation (3) can be expanded in a series [11,28,29],

$$S_y(\omega)/S_x(\omega) = \sum_{n,m=0}^{\infty} \tilde{A}^n \tilde{A}^m \mathbf{W}^n (\mathbf{W}^T)^m. \quad (4)$$

The cross spectra are normalized by  $S_x(\omega)^{-1}$  to obtain a unitless measure of network coherence, which we can use to approximate the average correlation coefficient (see [29]).

As shown by [11,28], the sum in Eq. (4) represents contributions to the cross spectrum from paths (i.e., motifs) within the network. Several second-order motifs are shown in Fig. 1. For instance, the second-order term  $\tilde{A}\tilde{A}(\mathbf{W}\mathbf{W}^T)_{ij} = w^2|\tilde{A}|^2 \sum_k \mathbf{W}_{ik}^0 \mathbf{W}_{jk}^0$  counts all contributions to the cross spectrum of nodes  $i$  and  $j$  due to common input from nodes  $k$  [the rightmost motif in Fig. 1(b)]. In general,  $(\mathbf{W}^n (\mathbf{W}^T)^m)_{ij}$  represents the contribution of  $(n,m)$  motifs which consist of two directed chains of length  $n$  and  $m$  emanating from a single apex and terminating in nodes  $i$  and  $j$ , respectively; see Fig. 2. The same node can be visited multiple times, and the  $(0,m)$  motif is a chain of length  $m$ .

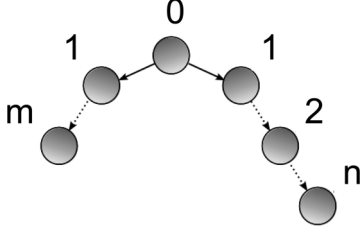

 FIG. 2. Illustration of an  $(n,m)$  motif.

Figure 3 illustrates such an expansion for two mutually inhibiting nodes (see also [28]). The cross covariance between the nodes is shown in Fig. 3(a) with contributions of low-order motifs in Fig. 3(b). As motif order increases, corresponding contributions to the cross covariance decrease in magnitude, but increase in width. The asymmetry of a contribution increases with the asymmetry of the associated motif, i.e., the difference between  $n$  and  $m$  in an  $(n,m)$  motif: Compare the contributions of the  $(1,2)$  and  $(0,3)$  motifs. A graphical decomposition of the circuit into the first few  $(n,m)$  motifs is shown in the inset of Fig. 3(b). Since the network is recurrent, the expansion in Eq. (4) does not terminate, as a node can appear multiple times in a motif.

### III. MOMENTS, CUMULANTS, AND NETWORKWIDE COHERENCE

We next relate network coherence and network structure using motif statistics. For concreteness—but without loss of generality [11,28]—we consider the total covariance between pairs of nodes. This is equivalent to evaluating all spectral quantities at  $\omega = 0$ , and we indicate this by suppressing dependences on  $\omega$ . We measure networkwide coherence using the average of this total covariance over all pairs of nodes. As in [11,28,29], if we denote by  $\langle \mathbf{X} \rangle$  the empirical average of the entries of matrix  $\mathbf{X}$ , we obtain, from Eq. (4),

$$\begin{aligned} \langle S_y \rangle / S_x &= \sum_{n,m=0}^{\infty} \tilde{A}^{n+m} \langle \mathbf{W}^n (\mathbf{W}^T)^m \rangle \\ &=: \frac{1}{N} \sum_{n,m=0}^{\infty} g^{n+m} \mu_{n,m} \quad \text{where } g = N \tilde{A} w. \end{aligned} \quad (5)$$

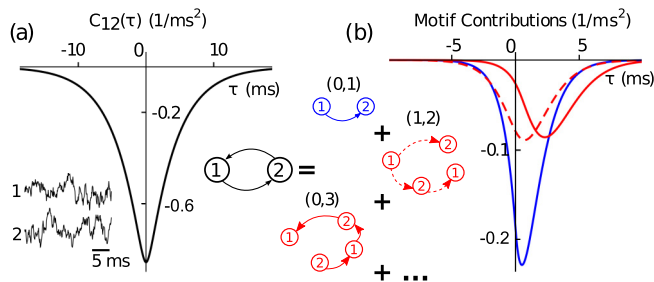


FIG. 3. (Color online) (a) The cross-correlation function of two mutually inhibiting nodes modeled by an Ornstein-Uhlenbeck process; inset shows traces of  $y_1(t)$  and  $y_2(t)$ . (b) Contribution of first- and third-order motifs to the cross-correlation function in (a). Middle inset: Diagrammatic expansion of the network showing motifs whose contributions are given, via the same line and color types, in (b).

Here the *motif moment*,  $\mu_{n,m} = \langle \mathbf{W}^{0n} (\mathbf{W}^{0T})^m \rangle / N^{n+m-1}$ , is the empirical probability of observing an  $(n,m)$  motif in the network [11,29]. Note that the empirical average is defined over a particular realization of the adjacency matrix  $\mathbf{W}^0$ . We define  $\mu_{n,0} = \mu_n$ , and let  $\mu_{0,0} = 1$ . The entire hierarchy of motif moments,  $\mu_{n,m}$ , needs to be known to evaluate Eq. (5) exactly. In practice, only a subset of  $\mu_{n,m}$ , up to a certain order  $n+m \leq k_{\max}$ , is known and can be used with Eq. (5) to approximate networkwide covariance.

Truncating Eq. (5) at some order yields an approximation of average coherence in terms of motif moments up to that order. However, these approximations can exhibit significant deviations from the true value [29]. Previously, we introduced an alternative, “motif resumming approximation” [29], which provided a series expansion of average coherence in terms of motif *cumulants* (defined below) rather than motif moments. Truncation of the resulting series yielded a significantly improved approximation of average coherence, given the same set of motif frequency data.

While we earlier provided a probabilistic interpretation of this motif cumulant approach, a general framework was missing [29]. We next provide such a framework by reexamining the motif cumulants  $\kappa_{n,m}$  that first appeared in [29]. We provide a definition which clarifies the underlying combinatorial relationship between motif cumulants  $\kappa_{n,m}$  and motif moments  $\mu_{n,m}$ , analogous to that between cumulants and moments of a random variable. Equipped with this definition, we are able to express dynamical correlations of all orders in terms of motif cumulants (Sec. V).

The construction of motif moments from cumulants is based on a familiar interpretation: estimating the probability of a joint event from the probability of its constituents. Figure 4(a) demonstrates this for an example motif. Each term in the decomposition of this  $(2,1)$  diverging motif arises from a cumulant of smaller or equal order. The first term corresponds to the probability of the motif occurring in a network with edges chosen independently, i.e., an Erdős-Rényi network. Subsequent terms give corrections from excess occurrences of second- and third-order submotifs. Thus, each motif cumulant,  $\kappa_{n,m}$ , captures “pure” higher-order connectivity statistics. Such decomposition can also be expressed in combinatorial form. Let  $\mathcal{C}(n)$  be the set of all compositions (*ordered partitions*) of  $n$ . Then,

$$\begin{aligned} \mu_n &= \sum_{\{n_1, \dots, n_t\} \in \mathcal{C}(n)} \left( \prod_{i=1}^t \kappa_{n_i} \right), \quad (6) \\ \mu_{n,m} &= \sum_{\substack{\{n_1, \dots, n_t\} \in \mathcal{C}(n) \\ \{m_1, \dots, m_s\} \in \mathcal{C}(m)}}} \left( \prod_{i=2}^t \kappa_{n_i} \right) (\kappa_{n_1, m_1} + \kappa_{n_1} \kappa_{m_1}) \\ &\quad \times \left( \prod_{j=2}^s \kappa_{m_j} \right). \end{aligned} \quad (7)$$

In evaluating these terms, we set  $(\prod_{i=2}^t \kappa_{n_i}) = 1$  if  $t = 1$ .

Expressions (6) and (7) define the full set of  $\kappa_{n,m}$  recursively. These are related directly to coherent network dynamics in the theorem that follows.

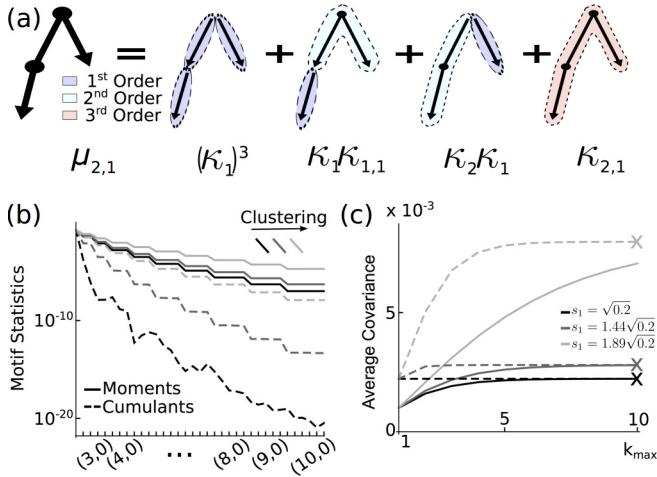


FIG. 4. (Color online) (a) The probability of observing the motif ( $\mu_{2,1}$ ) decomposed in terms of *motif cumulants* of the graph. (b) The magnitude of motif cumulants (dashed lines) and moments (solid lines) for stochastic block networks with  $N = 1000$ ,  $p = 0.2$ . Clustering in network connectivity increases from darker to lighter lines [see text for definition of clustering and network structure; precise values as specified in (c)]. The  $(n,m)$  motifs with  $n \geq m$  are listed first by order  $n + m$  then arranged by increasing  $n$  within the motifs of the same order. (c) Approximations of average covariances using motif moments [Eq. (5)] and cumulants [Eq. (8)] truncated at order  $k_{\max}$ . Crosses indicate exact values obtained from Eq. (3).

*Theorem 1.* For a network with dynamics defined by Eq. (1), with  $\mathbf{W} = w\mathbf{W}^0$ , the mean coherence (i.e., averaged across all cell pairs) is given by

$$\frac{\langle \mathbf{S}_y \rangle}{S_x} = \frac{1}{N} \left( 1 - \sum_{n=1}^{\infty} g^n \kappa_n \right)^{-2} \left( 1 + \sum_{n,m=1}^{\infty} g^{n+m} \kappa_{n,m} \right), \quad (8)$$

where  $g = N\tilde{A}w$ . The  $\kappa_{n,m}$  here are the motif cumulants, defined by (6) and (7).

To prove this result, we demonstrate a relation between the cumulants,  $\kappa_{n,m}$ , and the quantities expressed in terms of matrix products in Eq. (32) of [29]. Equation (8) then follows immediately from substituting the  $\kappa_{n,m}$  into Eq. (32) of [29]. The proof is given in the Appendix, Sec. 4.

In Fig. 4(c), we compare the expressions for network coherence in terms of motif moments [Eq. (5)] and motif cumulants [Eq. (8)]. We compute both expansions for three example networks (whose construction and differences will be the topic of later sections); for each, we illustrate how motifs of increasing order contribute to predicted network coherence.

This illustrates a general phenomenon. Truncating Eq. (5) and keeping only terms with  $n + m \leq k_{\max}$  approximates the contributions of these  $(n,m)$  motifs to the mean dynamical coherence in the network. A similar truncation of Eq. (8), however, approximates coherence in terms of contributions of paths of *all* orders. In this latter case, frequencies of motifs of order exceeding  $k_{\max}$  are *predicted* from the observed frequencies of motifs of order up to  $k_{\max}$ . Figure 4(c) shows that these predictions are useful: values of correlations based on cumulants converge more quickly than those derived from motif moments. The difference can be explained by looking at

the magnitude of the cumulants or moments against the order [Fig. 4(b)]. Importantly, cumulants decay much faster than moments in all three cases—hence the increased accuracy of Eq. (8) over Eq. (5) at a given order.

Figure 4(b) also illustrates that heterogeneity in network architecture can impact how quickly cumulants and moments decay, an observation we will revisit. The networks used in Figs. 4(b) and 4(c) have a variable degree of *clustering* or “clumping” in network connectivity—we precisely define our graph generation rules below. A greater degree of clustering results in a slower decay of both motif moments and cumulants. Higher-order statistics are necessary to accurately describe the structure of such networks. Hence, with more heterogeneity in connections across a network, the frequency of larger, more complex graph motifs has a greater impact on network coherence.

#### IV. HETEROGENEOUS NETWORKS AND SUBPOPULATION CUMULANTS

Motif cumulants—via Eq. (8)—provide a way to estimate global dynamical correlation in terms of local network structure. As illustrated above, the accuracy of such approximations depends on the network’s architecture (see Fig. 4). We next highlight the key impact of heterogeneity or clustering in network connectivity on the approximation. We then introduce a partitioning approach, and the allied concept of subpopulation cumulants, which allow us to relate local network structure to dynamics even in heterogeneous networks.

##### A. Heterogeneity in network architecture

To study the impact of heterogeneity on the approximation given by the motif cumulant method, we first consider the *stochastic block network model* [38–40] illustrated in Fig. 1. Such networks are comprised of two subpopulations (or clusters) of size  $N/2$  (indicated by circular and triangular nodes). Each cluster is associated with a constant  $s_i$ ,  $i = 1, 2$ , and the connection probability between nodes in subpopulation  $i$  and  $j$  is  $p_{ij} = s_i s_j$ . With fixed overall connection probability  $p$ , the difference between  $s_1$  and  $s_2$  describes the degree of clustering in the network. The case  $s_1 = s_2$  corresponds to an Erdős-Rényi network (no clustering), while  $s_1 = 2\sqrt{p}$ ,  $s_2 = 0$  implies that only nodes in the first subpopulation are connected (extremal clustering).

To illustrate the impact of clustering, we generate three networks with different values of  $s_1, s_2$  in Figs. 4(b) and 4(c). Comparing pairs of curves (moments and cumulants) with different shades (i.e., different degrees of clustering) reveals the dependence of motif moments and cumulants on graph structure. The magnitude of motif moments and cumulants of a given order increases with clustering [Fig. 4(b)]. Hence, in clustered, heterogeneous networks, large motifs can strongly impact dynamical coherence [Fig. 4(c)]. Moreover, network motifs of increasing order are needed to accurately predict dynamical correlations as clustering increases.

As a more complex example, we also considered the Barabási-Albert model. We find that the behavior of the two models is similar (Fig. 8 in the Appendix). Such similarity is consistent with observations reported in the literature [41]

and underscores the generality of the impact of network heterogeneity.

These results agree with intuition. Erdős-Rényi networks have an architecture that is “statistically homogeneous,” as the probability of each link occurring in the network is the same. Thus, the most local network statistic—connection probability—fully determines graph structure and hence the level of dynamical coherence. Similarly, “nearly Erdős-Rényi” networks are without significant graphical heterogeneity, and low-order motif cumulants can accurately predict dynamical coherence. On the other hand, in highly clustered networks, the probability of a path between a set of nodes depends on higher-order connectivity statistics. As a result, the frequency of large motifs cannot be obtained accurately from the frequencies of smaller ones. In such networks, higher-order motif statistics have a significant impact on dynamical coherence.

The necessity of estimating the frequency of higher-order motifs could limit the applicability of this approach. In many situations, the full connectivity structure of a network is not known and global properties of the network are difficult to estimate. For instance, in the case of biological neuronal networks, the number of neurons which can be simultaneously recorded in order to map out their connectivity is often limited to only a small handful [2,3]. Moreover, many networks possess additional structure past the simple heterogeneities discussed above—for instance, neuronal networks may be composed of both excitatory and inhibitory cells. Accounting

for such natural subdivisions of the graph can lead to more accurate approximations of dynamical coherence.

### B. Subpopulation cumulants

We next show how to subdivide a network to tame the effects of heterogeneity in architecture and reestablish the link between local connectivity and global coherence. Subsets of nodes in graphs can be grouped into classes, or subpopulations, that share features of dynamics or connectivity. Once a division is given, we can characterize each subpopulation by its own motif statistics. These subpopulation motifs are first introduced in [29] in the context of studying neural networks with two different types of cells. However, a key difference here is that division or grouping of nodes may not be given in advance, but can be obtained (as we will show) from the network architecture. How the nodes are subdivided can affect the accuracy of the motif cumulant method, which is a matter we will address in the next section. First, we extend the ideas in [29] to the general case of  $b$  populations using the combinatorial definition of motif cumulants introduced in Sec. III.

For  $b$  subpopulations,  $\boldsymbol{\mu}_{n,m}$  becomes a  $b \times b$  matrix of motif moments. Entry  $p,q$  of this matrix is the empirical probability of an  $(n,m)$  motif with end nodes belonging to populations  $p$  and  $q$ , respectively. Let  $V$  be the set of all nodes, and  $V_\alpha$ ,  $\alpha = 1, \dots, b$ , be the set of nodes in population  $\alpha$ . We denote the size of each population by  $N_\alpha = |V_\alpha|$ . We then have

$$\begin{aligned} (\boldsymbol{\mu}_{n,m})_{p,q} &= \sum_{i_n, i_{n-1}, \dots, i_0 \in V_p, j_1, \dots, j_{m-1}, j_m} \mathbf{W}_{i_n, i_{n-1}}^0 \mathbf{W}_{i_{n-1}, i_{n-2}}^0 \cdots \mathbf{W}_{i_1, i_0}^0 \mathbf{W}_{j_1, i_0}^0 \cdots \mathbf{W}_{j_{m-1}, j_m}^0 / Z \\ &= \sum_{i_n, i_{n-1}, \dots, i_0 \in V_p, j_1, \dots, j_{m-1}, j_m} \mathbf{W}_{i_n, i_{n-1}}^0 \mathbf{W}_{i_{n-1}, i_{n-2}}^0 \cdots \mathbf{W}_{i_1, i_0}^0 \mathbf{W}_{i_0, j_1}^{0T} \cdots \mathbf{W}_{j_{m-1}, j_m}^{0T} / Z \\ &= [(\mathbf{W}^0)^n (\mathbf{W}^{0,T})^m]_{p,q} / N^{n+m-1}. \end{aligned} \quad (9)$$

In these sums, we assumed that the indices satisfy  $i_n \in V_p$ ,  $j_m \in V_q$ , and other  $i_{s < n}$ ,  $j_{t < m}$  are chosen from  $V$ . We also used the normalization factor  $Z = N^{n+m-1} N_p N_q$ , while  $\langle \mathbf{M} \rangle_B$  represents the block average of a matrix according to the division of populations, i.e.,  $(\langle \mathbf{M} \rangle_B)_{p,q} = \frac{1}{N_p N_q} \sum_{i \in V_p, j \in V_q} M_{i,j}$ .

This partition of nodes and motifs into subpopulations is depicted in Fig. 1, where the color of a node indicates its class. Motifs may involve either nodes of a single class or a combination of the two.

Motif cumulants  $\boldsymbol{\kappa}_{n,m}$  are  $b \times b$  matrices that are defined by recursive relationships similar to Eqs. (6) and (7):

$$\boldsymbol{\mu}_n = \sum_{\{n_1, \dots, n_t\} \in \mathcal{C}(n)} \left[ \left( \prod_{i=2}^t \boldsymbol{\kappa}_{n_i} \mathbf{E} \right) \boldsymbol{\kappa}_{n_1} \right], \quad (10)$$

$$\boldsymbol{\mu}_{n,m} = \sum_{\substack{\{n_1, \dots, n_t\} \in \mathcal{C}(n) \\ \{m_1, \dots, m_s\} \in \mathcal{C}(m)}} \left( \prod_{i=2}^t \boldsymbol{\kappa}_{n_i} \mathbf{E} \right) (\boldsymbol{\kappa}_{n_1, m_1} + \boldsymbol{\kappa}_{n_1} \mathbf{E} \boldsymbol{\kappa}_{m_1}^T) \left( \prod_{j=2}^s \mathbf{E} \boldsymbol{\kappa}_{m_j}^T \right). \quad (11)$$

Here  $\mathbf{E} = \text{diag}\{N_1/N, \dots, N_b/N\}$  is inserted between each motif cumulant matrix multiplication and yields the appropriate weighted sums for the interpretation of the terms  $\boldsymbol{\mu}_{n,m}$  and  $\boldsymbol{\kappa}_{n,m}$  as *probabilities*. Specifically, scaling by  $\mathbf{E}$  is multiplication by the probability of selecting nodes from respective populations at “breaks” in the motifs.

How should these population-specific motif cumulants be combined to estimate the average correlation? An extension of

Eq. (8) was developed for two populations in [29], and stated in terms of matrix products. This generalizes immediately to the case of an arbitrary number of populations,  $b$ , and—as in Theorem 1 above—can be restated in terms of (matrix-valued) motif cumulants. The result is the following:

*Corollary 1.* Let  $\langle \mathbf{S}_y \rangle_B$  represent a blockwise average over entries corresponding to each subpopulation. For a network with dynamics defined by Eq. (1) with  $\mathbf{W} = w \mathbf{W}^0$ , the

generalization of Eq. (8) to subpopulation motif cumulants is [29]

$$\begin{aligned} \langle \mathbf{S}_y \rangle_B / S_x &:= \mathbf{D} \mathbf{U}^T \mathbf{S}_y \mathbf{U} \mathbf{D} / S_x \\ &= \frac{1}{N} \left( \mathbf{I} - \sum_{n=1}^{\infty} g^n \boldsymbol{\kappa}_n \mathbf{E} \right)^{-1} \left( \mathbf{E}^{-1} + \sum_{n,m=1}^{\infty} g^{n+m} \boldsymbol{\kappa}_{n,m} \right) \\ &\quad \times \left( \mathbf{I} - \sum_{m=1}^{\infty} g^m \mathbf{E} \boldsymbol{\kappa}_m^T \right)^{-1}, \end{aligned} \quad (12)$$

where  $\mathbf{D} = \text{diag}\{1/\sqrt{N_1}, \dots, 1/\sqrt{N_b}\}$ ,  $\mathbf{U}$  is the  $N \times k$  matrix given by  $\mathbf{U} = [\mathbf{u}_1 | \dots | \mathbf{u}_k]$ , and  $\mathbf{u}_i = (0, \dots, 0, 1, \dots, 1, 0, \dots, 0)^T / \sqrt{N_i}$  is the vector where the nonzero entries appear only at indices that match one of the nodes in the given subpopulation, normalized to unit  $L_2$  norm. The  $\boldsymbol{\kappa}_{n,m}$  here are the subpopulation motif cumulants, defined in Eqs. (10) and (11).

The arguments necessary to establish this corollary are given in the Appendix, Sec. 6.

In Fig. 5(a), we use stochastic block model networks to demonstrate the subpopulation motif approach. The structure of such networks is defined using two groups of nodes with different connectivity. We group nodes accordingly into two populations and apply the subpopulation cumulant formula given by Eq. (12). The resulting approximation of average correlations is a significant improvement over that obtained using a single population: First-order motif cumulants *alone* perfectly predict average correlations, whereas we require motifs of order up to four or five orders for the same networks if we use a single population approach [Fig. 4(b)].

Importantly, the subpopulation approach also works when there is no obvious way to group the nodes. As an example, consider the highly heterogeneous Barábasi-Albert networks. If we order nodes by degree, two subpopulations can be formed from nodes with degrees above and below a given threshold. Figure 5(b) shows that this approach substantially simplifies the link between network structure and dynamics: if the subpopulations are chosen optimally, covariance in the network dynamics can be accurately predicted using motifs of

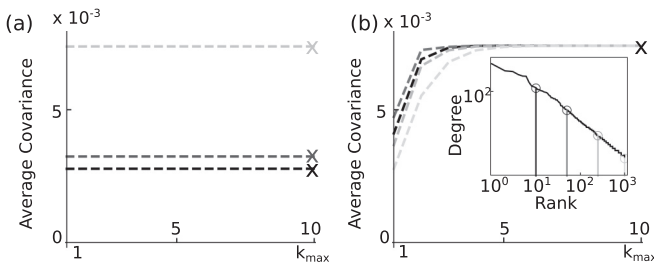


FIG. 5. Approximations of average covariances using the subpopulation cumulant approach, truncating at order  $k_{\max}$ . Crosses indicate exact values obtained from Eq. (3). (a) Stochastic block model networks of Fig. 4 (same color scheme) divided into two subpopulations—first-order motif cumulants now provide a complete description of the network structure; (b) Barábasi-Albert network divided into two subpopulations according to whether the sum of the in and out degrees of each node lies above or below different thresholds [inset shows cut-off degree ranks (descending)].

only order two, while motifs up to order four or five are needed otherwise.

### C. How to partition a network and why it works

In [29], we provided an intuitive explanation of why motif cumulants provide a better approximation of networkwide covariance [Eq. (8)] than motif moments [Eq. (5)]. In this section, we extend this argument to heterogeneous architectures. In doing so, we will reveal why network partitioning can work so well, describe a rule of thumb, and apply it to a general network.

First, we review the arguments in [29] for statistically homogeneous (e.g., Erdős-Rényi) networks. The argument was based on studying the spectral radii  $\Psi(\mathbf{W}^0)$  and  $\Psi(\mathbf{W}^0 \boldsymbol{\Theta})$ , where  $\boldsymbol{\Theta} = \mathbf{I} - \mathbf{u} \mathbf{u}^T$  and  $\mathbf{u} = (1, \dots, 1)^T / \sqrt{N}$ . Using the matrix expression of motif statistics [see Appendix, Eqs. (A2)–(A4)], it is straightforward to see that those spectral radii are related to the asymptotic rate of decay of the moments,  $\mu_{n,m}$ , [11] and cumulants,  $\boldsymbol{\kappa}_{n,m}$ , respectively.

The faster decay of cumulants compared to moments is therefore reflected by  $\Psi(\mathbf{W}^0 \boldsymbol{\Theta})$  being much smaller than  $\Psi(\mathbf{W}^0)$ . This is indeed the case for networks with sufficiently “homogeneous” connectivity [29] (cf. [11]): For Erdős-Rényi networks, the spectrum of  $\mathbf{W}^0$  is characterized by a bulk part with many eigenvalues distributed over a region near 0 in the complex plane, and one single positive eigenvalue with much larger magnitude. This latter eigenvalue determines  $\Psi(\mathbf{W}^0)$  (from the Perron-Frobenius (PF) theorem [42]; cf. [43]) and therefore the rate of decay of the moments  $\mu_{n,m}$ . To study  $\Psi(\mathbf{W}^0 \boldsymbol{\Theta})$ , and therefore the rate of decay of the motif cumulants, we first define the “PF vector” as the eigenvector associated with the outlying eigenvalue of  $\mathbf{W}^0$  in an arbitrary network. For sufficiently homogeneous networks such as Erdős-Rényi networks, the PF vector is close to  $\mathbf{u}$  as a reflection of the underlying homogeneity. Note that multiplication by  $\boldsymbol{\Theta}$  essentially removes the eigenvalue associated to this vector from the spectrum of  $\mathbf{W}^0 \boldsymbol{\Theta}$ , since  $\mathbf{W}^0 \boldsymbol{\Theta} \mathbf{u} = \mathbf{W}^0 \mathbf{0} = 0$ . This leads to the significant reduction of  $\Psi(\mathbf{W}^0 \boldsymbol{\Theta})$  compared to  $\Psi(\mathbf{W}^0)$ .

To extend such intuition to heterogeneous networks, we need to answer two questions: First, what is the PF vector for heterogeneous networks? Second, how does dividing a network into subpopulations change the counterpart of  $\boldsymbol{\Theta}$  and the resulting spectrum?

We first observe that for many networks, the PF vector is approximately the (in)-degree list, denoted by  $\mathbf{d}$  (normalized to unit  $L_2$  norm). In particular, we have found numerically that this is the case for stochastic block models and the Barábasi-Albert networks we consider (see Fig. 11 in the Appendix). We will use this observation about the PF vector to make intuitive arguments below, but first pause to make some general, heuristic comments as to its possible justification. We begin by referring back to the case of Erdős-Rényi networks, where the PF vector is approximately proportional to the homogeneous vector  $\mathbf{u}$  as stated above; and for large matrices,  $\mathbf{u}$  will also be approximately proportional to the degree vector  $\mathbf{d}$  with small (relative) error. Now, looking at the ensemble average  $\mathbf{E}\{\mathbf{W}^0\} \propto \mathbf{u} \mathbf{u}^T$ , we observe that  $\mathbf{u}$  is the (exact) PF vector for this average matrix  $\mathbf{u} \mathbf{u}^T$ . Thus,

the PF vector for the ensemble average and for realizations of the adjacency matrices agree—although this relies on the probabilistic structure of the underlying random matrices in a much more complicated way than we attempt to describe. Next, for a more general graph model, consider an adjacency matrix with an ensemble average that can be written in rank-one form:  $\mathbf{E}\{\mathbf{W}^0\} = \mathbf{a}\mathbf{b}^T$  (where  $\mathbf{a}, \mathbf{b}$  are column vectors with non-negative entries). The PF vector for  $\mathbf{E}\{\mathbf{W}^0\}$  is  $\mathbf{a}$ ; moreover, this is once again proportional to the (average) in-degree list. An analogy with the Erdős-Rényi case suggests a possible reason as to why the PF vector for individual adjacency matrices  $\mathbf{W}^0$  is also found to be approximately proportional to  $\mathbf{d}$ —although this argument is not rigorous.

We now discuss how to use the fact that the PF vector  $\propto \mathbf{d}$  to best partition a network into subpopulations. Recall that the subpopulation theory can be viewed as formally substituting the scalar motif moment and cumulant quantities in the original theory with  $b \times b$  matrices [Eqs. (10)–(12)]. In [29], we showed that the matrix expressions for  $\kappa_{n,m}$  and  $\mu_{n,m}$  are given by Eqs. (A2)–(A4), where repetitive factors such as  $\mathbf{W}^0 \Theta_B$  appear in places of  $\mathbf{W}^0 \Theta$ . Here,  $\Theta_B$  is a block diagonal generalization of  $\Theta$  for the subpopulation approach. In particular,

$$\Theta_B = \begin{pmatrix} \Theta_1 & & \\ & \ddots & \\ & & \Theta_b \end{pmatrix}, \quad (13)$$

where each diagonal block corresponds to a subpopulation. Here,  $\Theta_i = \mathbf{I}_{N_i} - \mathbf{u}_{N_i} \mathbf{u}_{N_i}^T$  (where  $\mathbf{u}_{N_i} = (1, \dots, 1)^T / \sqrt{N_i}$ ) is an “original”  $\Theta$  matrix, simply defined with population size  $N_i$ .

Combining the above observations, we look for a partition of the network that will bring  $\mathbf{W}^0 \Theta_B \mathbf{d}$  as close to 0 as possible. First, consider the stochastic block model. Note that the  $\Theta_B$  we defined above will map to  $\mathbf{0}$  any vector that is piecewise constant over the indices of each subpopulation. Therefore, if we choose the network partition naturally provided by the stochastic blocks themselves, we obtain  $\mathbf{W}^0 \Theta_B \mathbf{d} = \mathbf{0}$ . As expected, this partitioning results in very rapid decay of motif cumulants, and hence an ability to predict network coherence using only low-order motif statistics [here, order 1; see Fig. 5(a)].

For the Barábasi-Albert network, there are no “natural” subpopulations, but partitioning still leads to a significant improvement in predictions of network coherence. In this case, continue to divide the network into just two subpopulations [Fig. 5(b)]. The goal is to perform this division so that it will minimize  $\|\mathbf{W}^0 \Theta_B \mathbf{d}\|_2$ . In practice, we instead consider the simpler question of minimizing  $\|\Theta_B \mathbf{d}\|_2$  as an approximation. As noted above,  $\|\Theta_B \mathbf{d}\|_2$  measures the error of a piecewise constant (over the indices of subpopulations) approximation of  $\mathbf{d}$ . In Fig. 6, we plot this error against a threshold parameter

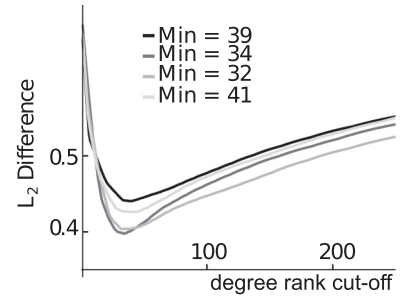


FIG. 6.  $L_2$  norm of the difference between the degree list (normalized) and the piecewise constant vector (see text) given by a certain cut-off ranking of the degrees. Curves with different shades are four realizations of Barábasi-Albert networks (with the same parameters). The legend is the cut-off degree ranking that achieves the minimum of difference.

in node degree that is chosen to partition the network; this shows that the error is minimized at a cut-off degree ranking of roughly 30–40 (across different random realizations of a Barábasi-Albert network with the same parameters). As expected from our heuristic arguments, this value is close to the value of the threshold that gave the most rapid convergence of the cumulant-based estimates of network covariance (degree ranking = 50; Fig. 6).

Up to this point, we have defined motif cumulants and shown how they can be used to make accurate predictions of coherence in average network activity. These were results about second-order correlations (i.e., covariances) averaged across node pairs. We next extend the theory of motif cumulants to correlations of arbitrary order.

## V. HIGHER-ORDER CORRELATIONS

Here we show how to generalize our theory to relate higher-order statistics of a network’s dynamics to its architecture. While the second-order results above can be used for both finite-valued stochastic systems (i.e., OU and jump processes) and coupled point processes, the higher-order results are *only valid in their present form for finite-valued stochastic systems* (not point processes with  $\delta$  function pulses). Extensions to higher-order coherence for interacting point processes are nontrivial and will be tackled elsewhere.

The  $k$ th-order cross-covariance function for the processes in Eq. (1) are defined using joint cumulants of random variables,

$$\begin{aligned} \mathbf{C}_{y^{[k]}^{i_1 i_2 \dots i_k}}(\tau_1, \dots, \tau_{k-1}) \\ := \kappa(y_{i_1}(t), y_{i_2}(t + \tau_1), \dots, y_{i_k}(t + \tau_{k-1})). \end{aligned} \quad (14)$$

A generalization of the Wiener-Khinchin theorem relates the Fourier transform of the higher-order cumulant to the polyspectra  $\mathbf{S}_{y^{[k]}^{i_1 i_2 \dots i_k}}$  [44] defined via the Fourier transform of the processes:

$$\begin{aligned} \mathcal{F}(\mathbf{C}_{y^{[k]}^{i_1 i_2 \dots i_k}}) &= \mathbf{S}_{y^{[k]}^{i_1 i_2 \dots i_k}} = \kappa(\tilde{y}_{i_1}(\omega_1 + \dots + \omega_{k-1}), \tilde{y}_{i_2}(\omega_1), \dots, \tilde{y}_{i_k}(\omega_{k-1})) \\ &:= \lim_{T \rightarrow \infty} \frac{1}{T} \sum_{\chi} (|\chi| - 1)! (-1)^{|\chi| - 1} \prod_{B \in \chi} \mathbf{E} \left\{ \prod_{j \in B} \tilde{y}_{i_j}(\omega_{j-1}) \right\} \delta \left( \sum_{j \in B} \omega_j \right). \end{aligned} \quad (15)$$

Here,  $\omega_0 = -\sum_{j=1}^{k-1} \omega_j$ ,  $\tilde{y}_{ij}(\omega) = \int_0^T dt e^{-2\pi i \omega t} (y_{ij}(t) - \mathbf{E}[y_{ij}(t)])$ , and  $\delta(z) = 1$  when  $z = 0$  and  $\delta(z) = 0$  otherwise. The first sum is over all partitions  $\chi$  of set  $\{1, \dots, k\}$ , and  $B$ , as an element of  $\chi$ , is a subset of  $\{1, \dots, k\}$ ;  $|\chi|$  is the number of partitions in  $\chi$ . To illustrate this formula, we first note that at third order, it reduces exactly to the ‘‘bispectrum’’ [44–46]

$$\begin{aligned} \mathcal{F}(\mathbf{C}_{y[3]}^{i_1 i_2 i_3}(\tau_1, \tau_2)) &= \mathbf{S}_{y[3]}^{i_1 i_2 i_3}(\omega_1, \omega_2) \\ &:= \mathbf{E}[\tilde{y}_{i_1}(\omega_1 + \omega_2) \tilde{y}_{i_2}(\omega_1) \tilde{y}_{i_3}(\omega_2)]. \end{aligned}$$

It is easy to see that Eq. (15) is multilinear in the variables  $\tilde{y}_{ij}$ . Using Eq. (2), we can therefore generalize Eq. (3) to obtain the polyspectra of the processes  $\mathbf{y}$  in terms of that for  $\mathbf{x}$  via the propagation matrix  $\tilde{\mathbf{P}} = (\mathbf{I} - \tilde{\mathbf{A}}\mathbf{W})^{-1}$ :

$$\begin{aligned} \mathbf{S}_{y[k]}^{i_1 i_2 \dots i_k}(\omega_1, \dots, \omega_{k-1}) &= \sum_{j_1, \dots, j_k} \tilde{\mathbf{P}}_{i_1 j_1}(\omega_0) \tilde{\mathbf{P}}_{i_2 j_2}(\omega_1) \dots \tilde{\mathbf{P}}_{i_k j_k}(\omega_{k-1}) \mathbf{S}_{x[k]}^{j_1 j_2 \dots j_k} \\ &\times (\omega_1, \dots, \omega_{k-1}). \end{aligned} \quad (16)$$

For example, replacing Gaussian white noise which appeared in the OU process with ‘‘Poisson kicks’’, i.e., considering a shot noise process, yields nonzero  $\mathbf{S}_{x[3]}$ .

Next, expanding  $\tilde{\mathbf{P}} = \sum_{n=0}^{\infty} (\tilde{\mathbf{A}}\mathbf{W})^n$  in Eq. (16) leads to an expression for polyspectra analogous to Eq. (5):

$$\langle \mathbf{S}_{y[k]} \rangle / S_{x[k]} = \frac{1}{N^{k-1}} \sum_{n_1, \dots, n_k=0}^{\infty} g^{|n|} \boldsymbol{\mu}_{n_1, \dots, n_k}, \quad (17)$$

where  $|n| = \sum_{i=1}^k n_i$  and  $g = N\tilde{\mathbf{A}}w$  as defined in Eq. (5). The motif moments  $\boldsymbol{\mu}_{n_1, \dots, n_k} = \sum_{i_1, \dots, i_k, j} (\mathbf{W}^{0n_1})_{i_1 j} \dots (\mathbf{W}^{0n_k})_{i_k j} / N^{|n|+1}$ . For simplicity, in the formula above, we again set  $\omega_1 = \dots = \omega_{k-1} = 0$ , and assume homogeneous dynamics for each node. Here,  $\mathbf{S}_{x[k]}^{i_1 i_2 \dots i_k} = S_{x[k]} \delta^{i_1 i_2 \dots i_k}$  is a diagonal tensor, since the  $\{x_i\}$  comprise an uncoupled and uncorrelated network.

The most interesting aspect of Eq. (17) is the motif moments  $\boldsymbol{\mu}_{n_1, \dots, n_k}$ . For dynamical coherence (and hence polyspectra) of order  $k$ , these motif moments are the frequencies of  $k$ -branch motifs with  $n_j$  nodes on each branch. Figure 7(a) illustrates such a motif  $\boldsymbol{\mu}_{1,1,1}$ , for  $k = 3$  branches and  $n_j \equiv 1$  node on each branch. Importantly, these  $k$ -branch motifs are the only ones that appear at each order in the series of Eq. (17).

We note that higher-order correlations for more general cases, such as variable connection weights, heterogeneity in node dynamics, and common input can be treated similarly, using techniques in [29].

Thus far, we have shown via Eq. (17) how network motifs—quantified by the motif moments  $\boldsymbol{\mu}_{n_1, \dots, n_k}$ —contribute to higher-order dynamical correlations. The solid lines in Fig. 7(b) show that the motif moments can decay slowly. The consequence is that motifs of high order (up to 10 or beyond) may be needed for a good approximation of third-order correlations [Fig. 7(c), solid lines].

It is therefore natural to ask whether the motif cumulant approach can be extended to higher order, and help approximate finer measures of coherence using information about only a few lower-order motifs. Although the main ideas are similar to those at second order, derivations at higher order are

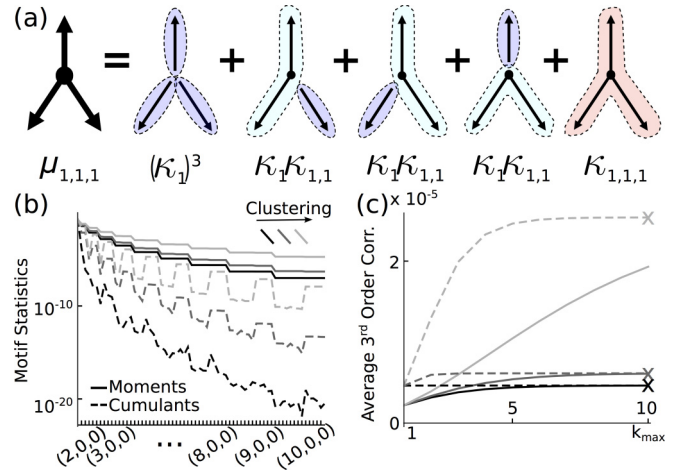


FIG. 7. (Color online) (a) Cumulant decomposition of a three-branch motif. Panels (b) and (c) are counterparts of Fig. 4(b) and 4(c) for three-branch motifs and bispectra: (b) decay of motif moments and cumulants with respect to order and (c) convergence estimated third-order correlations by two approaches. In (b), the  $(n, m, l)$  motifs are again increasingly ordered according to the order  $n + m + l$ . Because of symmetry, only motifs with  $n \geq m \geq l$  are listed. Within each order, motifs are arranged by lexicographical order of  $n, m$ , and  $l$ , except that motifs with  $l \neq 0$  are listed first.

more cumbersome. We note that a significant simplification is offered by the use of our combinatorial formulation of motif cumulants (Sec. III).

First, we define multibranch motif cumulants via their relationship with motif moments. Specifically, we relate the motif moments  $\{\boldsymbol{\mu}_*\}$  and motif cumulants  $\{\boldsymbol{\kappa}_*\}$  ( $*$  stands for multiple indices; see below) via a combinatorial expression. This expression corresponds to the decomposition shown in Fig. 7(a) [cf. Fig. 4(a)], where we have decomposed a  $k$ -branch motif into motifs with  $k$  and fewer branches.

We next enumerate all possible ways of decomposing the  $k$ -branch motif explicitly. Just as in Eqs. (6) and (7), this is done according to how a  $k$ -branch motif is partitioned at the ‘‘root’’ of the branches [the sum over  $\chi$  in Eq. (18)]. In other words, we examine which  $k$  branches are grouped together as one component in the decomposition. To see what this means, examine the coloring in Fig. 7(a): for different terms in the decomposition, the components that are shaded with the seam color have been grouped together. The remaining enumeration is about how each branch breaks up [into chains  $\boldsymbol{\kappa}_{B_j^i}$ , corresponding to the sum over  $\pi_i$  in Eq. (18)],

$$\boldsymbol{\mu}_{n_1, \dots, n_k} = \sum_{\pi_1, \dots, \pi_k} \left( \prod_{i=1}^k \prod_{j=2}^{t_i} \boldsymbol{\kappa}_{B_j^i} \right) \left( \sum_{\chi} \prod_{\{i_1, \dots, i_s\} \in \chi} \boldsymbol{\kappa}_{B_{i_1}^{i_1}, \dots, B_{i_s}^{i_s}} \right). \quad (18)$$

Here,  $\pi_i = \{B_1^i, \dots, B_{t_i}^i\}$  is an ordered partition of  $n_i$ ,  $\chi$  is a partition of the set  $\{1, \dots, k\}$ , and  $\{i_1, \dots, i_s\}$  is one subset of indices that are grouped according to the partition  $\chi$ .

To generalize Eq. (8), we use the following analog of Prop. 4.1 in [29].



*Theorem 2.* For a pair of motif moments and cumulants  $\{\mu_*\}$  and  $\{\kappa_*\}$  with up to  $k$  branches,

$$\begin{aligned} & \sum_{n_1, \dots, n_k=0}^{\infty} \mu_{n_1, \dots, n_k} \\ &= \left(1 - \sum_{n=1}^{\infty} \kappa_n\right)^{-k} \\ & \times \left[ \sum_{\pi} f(\pi) \prod_{B \in \pi, B > 1} \left( \sum_{n_1, \dots, n_B=1}^{\infty} \kappa_{n_1, \dots, n_B} \right) \right], \end{aligned} \quad (19)$$

assuming all series converge absolutely and  $|\sum_{n=1}^{\infty} \kappa_n| < 1$ . The sum with index  $\pi$  is through all partitions of  $k$ . When indices for the product are empty, we take the corresponding terms to be 1. The Faà di Bruno coefficient,

$$f(\pi) = \left( \sum_{B \in \pi} B \right)! \left( \prod_{B \in \pi} B! \right)^{-1} \left( \prod_{B \in \pi} \#B! \right)^{-1}, \quad (20)$$

is the number of partitions of set  $\{1, \dots, k\}$  that correspond to a partition  $\pi$  of integer  $k$ . Here,  $v$  is the set of unique  $B$ 's in  $\pi$ , and for every  $B \in v$ ,  $\#B$  is the number of repetitions of  $B$  in  $\pi$ .

We provide a proof of Theorem 2 in the Appendix, Sec. 5, using the combinatorial relation given by Eq. (18). We note that the proof itself is different from the matrix-based method used in [29] to obtain the second-order correlation result. Moreover, this approach can be easily generalized to the case of subpopulations (see below and the Appendix, Sec. 6).

To establish an expression for average higher-order correlations, first note that Eq. (18) is “homogeneous in degree,” so that if it is satisfied for a pair of motif moments and cumulants  $\{\mu_*\}$ ,  $\{\kappa_*\}$ , it will also be satisfied for scaled pairs  $\{g^{|\mu_*|} \mu_*\}$ ,  $\{g^{|\kappa_*|} \kappa_*\}$ . Thus, the same relationship holds for scaled motif statistics. Applying Theorem 2 to Eq. (17), using scaled motif statistics, we obtain

$$\begin{aligned} \frac{\langle S_{y[k]} \rangle}{S_{x[k]}} &= \frac{1}{N^{k-1}} \left(1 - \sum_{n=1}^{\infty} g^n \kappa_n\right)^{-k} \\ & \times \left[ \sum_{\pi} f(\pi) \prod_{B \in \pi, B > 1} \left( \sum_{n_1, \dots, n_B=1}^{\infty} g^{|\mu_{n_1, \dots, n_B}|} \kappa_{n_1, \dots, n_B} \right) \right]. \end{aligned} \quad (21)$$

As an example, the motif cumulant expansion of the average third-order correlation is

$$\begin{aligned} \frac{\langle S_{y[3]} \rangle}{S_{x[3]}} &= \frac{1}{N^2} \left(1 - \sum_{n=1}^{\infty} g^n \kappa_n\right)^{-3} \\ & \times \left(1 + 3 \sum_{l,m=1}^{\infty} g^{l+m} \kappa_{l,m} + \sum_{l,m,n=1}^{\infty} g^{l+m+n} \kappa_{l,m,n}\right). \end{aligned} \quad (22)$$

Figures 7(b) and 7(c) are counterparts of Figs. 4(b) and 4(c) that numerically compare motif moment and cumulant approaches for stochastic block networks. They show numerically that our observations for pairwise correlations

generalize to higher orders (see also Fig. 9 in the Appendix for an application to the Barabási-Albert network). First, we show that higher-order correlations can depend on long paths through the network (motif moments, solid lines). Second, when predicting average correlation using motif statistics up to a given order, an approximation in terms of motif cumulants is more accurate than one in terms of motif moments [Fig. 7(c)]. Third, the order of motif statistics needed to approximate correlations again increases with network homogeneity (compare lines of different shade).

Finally, the subpopulation approach generalizes to higher order. The resulting general formula is given in Corollary 2 and derived in the Appendix, Sec. 7. Moreover, this result offers similar advantages in predicting correlations from lower-order motif cumulants (see the Appendix, Sec. 6, and Fig. 10).

## VI. CONCLUSION

Network motifs have been used previously to link local network connectivity and global coherence in networks with linearly interacting components [11,28,29]. Here, we developed this theory in order to make it both more general and more broadly applicable. We first showed that a motif-based approach introduced in prior work has a probabilistic interpretation in terms of quantities closely related to key statistical concepts. We refer to these as motif cumulants.

Next, we showed that the link between network architecture and dynamical correlation—through motif cumulants—can be *complex* in clustered and heterogeneous networks. This complexity can result in the apparently irreducible contribution of long paths to networkwide coherence. However, the motif cumulant approach can be extended to reduce this complexity—and hence the size and number of the network features that must be sampled empirically—substantially. Finally, we showed how the theory naturally extends to higher-order dynamical correlations for a broad subset of the dynamical models under study. This provides a direct link between local network architecture and global dynamics at every order.

An important feature of our approach for experimental settings is that the prevalence of only a limited number of motifs is needed in order to predict networkwide dynamical coherence. Moreover, these motifs are small, involving only a few nodes at a time. This property could provide a way forward in experimental settings—as in studies of networks of genes [47] or neurons [2,3]—in which networks are quantified by sampling a limited number of edges measured simultaneously. The resulting motif prevalences are precisely the quantities needed to define the motif cumulants that are at the core of our approach.

The present results suggest many opportunities for future research. At the top of the list is extending the connection between network motifs and higher-order dynamical correlations to apply to coupled point process models. Somewhat surprisingly, we have found both numerically and analytically (in special cases) that the linear response approach [Eq. (16)] that extends to all orders for finite-valued stochastic processes fails to extend beyond second order for coupled point process models, where each node generates “spike” events (data not shown). Future research will explore modifications of the linear response approach that may reestablish a useful

description of higher-order correlations for these network models. This would open the door to studies of plasticity and learning of network connections in neural systems, where interactions are governed by spike times [48].

We close by mentioning two further extensions of special interest. The first concerns applications to stimulus-encoding networks. Such networks can be heterogeneous and composed of groups of nodes, each with different connectivity rules and, importantly, responding differently to an external stimulus. Networks with spatial structure provide a natural way in which such connectivity and responses might develop. For such a network, our subpopulation motif approach could predict the levels of dynamical coherence within and between each group of nodes. From here, decoding techniques could quantify the level of information that the neural groups carry about the stimulus itself, and how this depends on the correlation structure induced by different network motifs [20–25,49,50].

A final open problem concerns the invertibility of the architecture-to-dynamics question considered here. Given measurements of networkwide coherence, what can we conclude about network architecture? The network motif approach can narrow the possibilities, especially when higher-order correlations are considered, but we do not yet know what additional assumptions are required to yield a unique solution.

#### ACKNOWLEDGMENTS

We thank C. Hoffman, K. Bassler, and B. Doiron for helpful insights and suggestions. This work was supported by NSF Grant No. DMS-1122094, a joint NSF/NIGMS Grant No. R01GM104974, a Texas NHARP award to K.J., and a Career Award at the Scientific Interface from the Burroughs Wellcome Fund and NSF Grants No. DMS-1056125 and No. DMS-0818153 to ESB.

#### APPENDIX

##### 1. Relating the Ornstein-Uhlenbeck model to Eq. (1) of the main text

We used a simplified form of the canonical Ornstein-Uhlenbeck (OU) model in all examples where we consider second-order statistical quantities. This model is related to Eq. (1) in the main text by writing the dynamics

$$\dot{\mathbf{y}} = -\mathbf{\Lambda}\mathbf{y}(t) + \mathbf{W}\mathbf{y}(t) + \boldsymbol{\xi}(t), \quad (\text{A1})$$

where  $\mathbf{y}(t) = [y_1(t), \dots, y_N(t)]^T$ . The diagonal matrix  $\mathbf{\Lambda} = \tau^{-1}\mathbf{I}$  sets the intrinsic time scale of the nodes, and the column vector  $\boldsymbol{\xi}(t)$  is composed of independent white noise processes. Equation (A1) above is then equivalent to Eq. (1) of the main text with  $A_i(t) = A(t) = e^{-t/\tau}\Theta(t)$ . Upon coupling, the baseline activity of a node in the network,  $\mathbf{x}_i(t) = (A * \boldsymbol{\xi})(t)$ , is perturbed by filtered input from other nodes,  $A * \sum_j \mathbf{W}_{ij}y_j(t)$ .

##### 2. Further examples

Here we provide details of several computational findings referred to in the main text. Each addresses the generality and applicability of our results. First, Fig. 8 shows that our main results contrasting motif moments and cumulants hold for the Barabási-Albert network model, which has a significantly

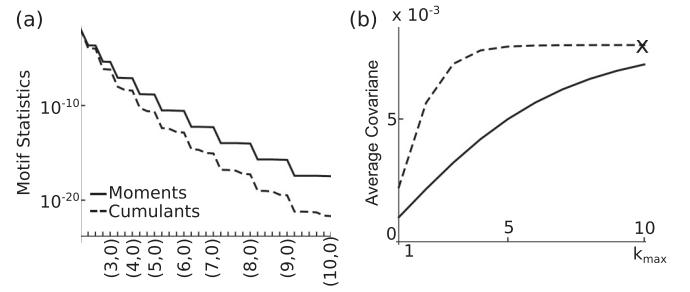


FIG. 8. Same as Figs. 4(b) and 4(c) of the main text but for the Barabási-Albert model. (a) The magnitude of motif cumulants (dashed lines) and moments (solid lines) for a Barabási-Albert model network. Motifs  $(n,m), n \geq m$  are grouped first by  $n+m$  and then arranged by increasing  $n$ . (b) Approximations of average covariances using motif moments [truncating Eq. (5), solid lines] and cumulants [truncating Eq. (8), dashed lines] up to order  $k_{\max}$ . Exact values [direct evaluation of Eq. (3)] are labeled by crosses: a Barabási-Albert network of size 1000 and connection probability 0.01.

more complex structure than the stochastic block models studied in Fig. 4 of the main text.

Next, Figs. 9 and 10 present analogous results for third-order correlations in network output. Specifically, Fig. 9 shows that these third-order correlations depend significantly on the details of the underlying graph structure (i.e., the degree of clustering). Moreover, this dependence can be efficiently predicted via motif cumulants. Figure 10 demonstrates that the subpopulation approaches continue to enhance the accuracy of our predictions—if the populations are correctly defined, levels of triplet correlations can be predicted from lower-order motifs.

Figure 11 provides numerical evidence for our claim that the PF vector for a general class of networks is closely approximated by the degree list (see Sec. IV C).

##### 3. Details of numerical results

Here we provide a detailed description of the computational examples in the main text and the Appendix. This includes all parameters describing the dynamics of nodes and connections, and our methods of generating random networks.

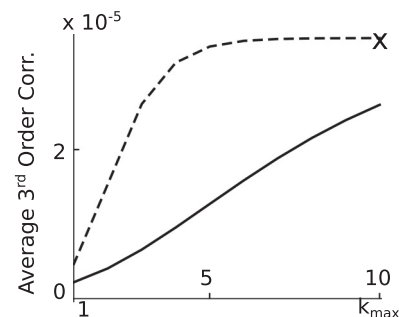


FIG. 9. Same plot as Fig. 8(b) but for average third-order correlations  $\langle S_{y[3]} \rangle / S_{y[3]}$ . Approximations using motif moments (solid lines) and cumulants (dashed lines) up to order  $k_{\max}$  for a Barabási-Albert network of size 1000 and connection probability 0.01.

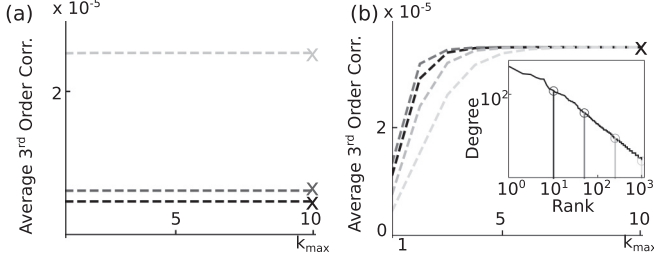


FIG. 10. Same plots as Fig. 5 of the main text but for average third-order correlations  $\langle \mathbf{S}_{y[3]} \rangle / S_{x[3]}$ . Approximations using the subpopulation cumulant approach by truncating at order  $k_{\max}$ , with the exact values [direct evaluation of Eq. (16) of the main text] labeled by crosses: (a) stochastic block model networks of Fig. 4 of the main text (the colors are the same) divided into two subpopulations with differing connectivities; (b) the Barabasi-Albert network of Fig. 8 divided into two subpopulations according to different thresholds on the sum of the in and out degrees (different colors; see also the inset, which displays the cutoffs).

In Fig. 3 of the main text, we calculated correlations for an OU system [see Eq. (A1) of the main text] with  $\tau = 1$ ,  $\xi$  having unit intensity, and

$$\mathbf{W} = \begin{bmatrix} 0 & -0.75 \\ -0.75 & 0 \end{bmatrix}.$$

In plots of approximations of average second- and third-order covariances, i.e., Figs. 4(b), 5(a) and 5(b) of the main text, as well as Figs. 8(b), 9, 10(a), and 10(b), the parameters  $\bar{A}$  and  $w$  are chosen so that  $N\bar{A}wp = 0.4$ . Note that the choice of  $S_x$  (respectively,  $S_{x[3]}$  at third order) will not affect the normalized quantity  $\langle \mathbf{S}_y \rangle / S_x$  (respectively,  $\langle \mathbf{S}_{y[3]} \rangle / S_{x[3]}$ ), and can be set to 1.

The Barabasi-Albert networks in Fig. 5(b), and Figs. 8(a), 8(b), 9, and 10(b), are generated by a directed Barabasi-Albert model similar to that in [41]. One starts with a “core” of  $Np$  nodes, randomly connected with connection probability 0.5. After that,  $N - Np$  nodes are added to the graph. When adding a new node  $i + 1$ , it will form exactly  $Np$  connections with the existing nodes  $1, \dots, i$ . Those connections are distributed among existing nodes according to probabilities that are proportional to the sum of the in and out degree of each node. The direction of the connection, whether into node  $i + 1$  or

out of node  $i + 1$ , is chosen independently with probability 0.5. The code implementing this algorithm is available upon request.

#### 4. Explicit expressions for motif cumulants

Here, we will prove that the following matrix expressions for  $\kappa_n$  and  $\kappa_{n,m}$  introduced in [29] are equivalent to the recursive definition in Eqs. (6) and (7) of the main text:

$$\begin{aligned} \kappa_n &= \frac{1}{N^{n+1}} \sum_{i,j} \underbrace{(\mathbf{W}^0 \Theta \mathbf{W}^0 \dots \Theta \mathbf{W}^0)_{ij}}_{n \text{ factors of } \mathbf{W}^0} \\ &= \frac{1}{N^n} \mathbf{u}^T [(\mathbf{W} \Theta)^{n-1} \mathbf{W}] \mathbf{u} \\ &= \frac{1}{N^n} \mathbf{u}^T \mathbf{W}_n^\theta \mathbf{u}, \end{aligned} \quad (\text{A2})$$

$$\begin{aligned} \kappa_{n,m} &= \frac{1}{N^{n+m+1}} \\ &\times \sum_{i,j} \underbrace{(\mathbf{W}^0 \Theta \mathbf{W}^0 \dots \Theta \mathbf{W}^0)_{ij}}_{n \text{ factors of } \mathbf{W}^0} \underbrace{(\mathbf{W}^0 \Theta^T \Theta \mathbf{W}^0 \dots \Theta \mathbf{W}^0)_{ij}}_{m \text{ factors of } \mathbf{W}^{0T}} \\ &= \frac{1}{N^{n+m}} \mathbf{u}^T [(\mathbf{W} \Theta)^{n-1} \mathbf{W} \Theta \mathbf{W}^T (\Theta \mathbf{W}^T)^{m-1}] \mathbf{u} \\ &= \frac{1}{N^{n+m}} \mathbf{u}^T \mathbf{W}_n^\theta \Theta \mathbf{W}_m^\theta \mathbf{u}, \end{aligned} \quad (\text{A3})$$

where

$$\mathbf{W}_n^\theta = [\mathbf{W}^0 \Theta]^{n-1} \mathbf{W}^0$$

and  $\mathbf{u} = (1, \dots, 1)^T / \sqrt{N}$ ,  $\mathbf{H} = \mathbf{u} \mathbf{u}^T$ , and  $\Theta = \mathbf{I} - \mathbf{H}$ .

We see that  $\mathbf{W}^0 \Theta$ ,  $\Theta \mathbf{W}^T$  are recurring factors in  $\kappa_n$  and  $\kappa_{n,m}$ . Using the relation of spectral radius and matrix norm [11], one can show that the asymptotic decay speed of  $\kappa_*$  is determined by the spectral radii of these factors. Interestingly, it is easy to show that  $\Psi(\mathbf{W}^0 \Theta) = \Psi(\Theta \mathbf{W}^0 \Theta) = \Psi(\Theta \mathbf{W}^0)$ , and hence these spectral radii coincide. A similar argument relates the decay of  $\mu_*$  with  $\Psi(\mathbf{W}^0)$  [Eq. (A4)].

We prove only that Eq. (A3) holds, since a nearly identical, but simpler, proof verifies Eq. (A2). First, recalling that  $\mu_{n,m} = \langle \mathbf{W}^{0n} (\mathbf{W}^{0m})^T \rangle / N^{n+m-1}$ , it is straightforward to show

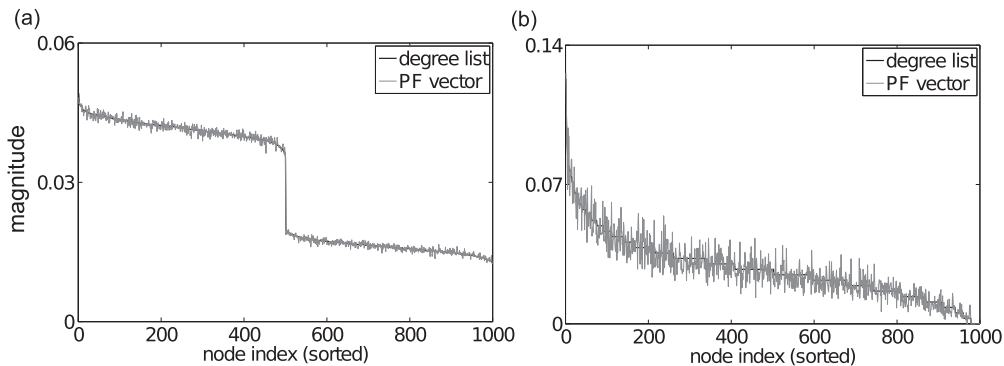


FIG. 11. Comparing the PF vector (gray) and the in-degree list (black) for (a) a stochastic block network and (b) a Barabasi-Albert network. The vectors are normalized to have unit  $L_2$  norm and plotted by the indices of nodes, which are ordered in descending in-degree. The stochastic block network has  $s1 = 1.44\sqrt{0.2}$  and is the same one as in Figs. 4(b) and 4(c). The Barabasi-Albert network is the same one as in Fig. 5(b).

that

$$\boldsymbol{\mu}_{n,m} = \frac{1}{N^{n+m}} \mathbf{u}^T (\mathbf{W}^0)^n (\mathbf{W}^{0T})^m \mathbf{u}. \quad (\text{A4})$$

Substituting  $\mathbf{I} = \boldsymbol{\Theta} + \mathbf{H}$  between every subsequent appearance of the adjacency matrix  $\mathbf{W}^0$  gives

$$\begin{aligned} \boldsymbol{\mu}_{n,m} &= \frac{1}{N^{n+m}} \mathbf{u}^T [\mathbf{W}^0 (\boldsymbol{\Theta} + \mathbf{H})]^{n-1} \mathbf{W}^0 (\boldsymbol{\Theta} + \mathbf{H}) \mathbf{W}^{0T} \\ &\quad \times [(\boldsymbol{\Theta} + \mathbf{H}) \mathbf{W}^{0T}]^{m-1} \mathbf{u}. \end{aligned} \quad (\text{A5})$$

By expanding across all sums of  $\boldsymbol{\Theta} + \mathbf{H}$  except the central one (between the terms  $\mathbf{W}^0, \mathbf{W}^{0T}$ ), and noting that there

is an obvious bijection between a pair of compositions of the integers  $n$  and  $m$ , i.e.,  $\{n_1, \dots, n_t\} \in \mathcal{C}(n), \{m_1, \dots, m_s\} \in \mathcal{C}(m)$ , and a term of the form

$$\left[ \prod_{i=1}^{t-1} (\mathbf{W}_{n_i}^\theta \mathbf{H}) \right] [\mathbf{W}_{n_t}^\theta (\boldsymbol{\Theta} + \mathbf{H}) \mathbf{W}_{m_s}^\theta] \left[ \prod_{j=1}^{s-1} (\mathbf{H} \mathbf{W}_{m_j}^\theta) \right],$$

we may write (using  $\mathbf{H} = \mathbf{u} \mathbf{u}^T$ )

$$\begin{aligned} \boldsymbol{\mu}_{n,m} &= \frac{1}{N^{n+m}} \mathbf{u}^T \left\{ \sum_{\substack{\{n_1, \dots, n_t\} \in \mathcal{C}(n) \\ \{m_1, \dots, m_s\} \in \mathcal{C}(m)}}} \left[ \prod_{i=1}^{t-1} (\mathbf{W}_{n_i}^\theta \mathbf{H}) \right] [\mathbf{W}_{n_t}^\theta (\boldsymbol{\Theta} + \mathbf{H}) \mathbf{W}_{m_s}^\theta] \left[ \prod_{j=1}^{s-1} (\mathbf{H} \mathbf{W}_{m_j}^\theta) \right] \right\} \mathbf{u} \\ &= \frac{1}{N^{n+m}} \sum_{\substack{\{n_1, \dots, n_t\} \in \mathcal{C}(n) \\ \{m_1, \dots, m_s\} \in \mathcal{C}(m)}}} \left[ \prod_{i=1}^{t-1} (\mathbf{u}^T \mathbf{W}_{n_i}^\theta \mathbf{u}) \right] [\mathbf{u}^T \mathbf{W}_{n_t}^\theta (\boldsymbol{\Theta} + \mathbf{u} \mathbf{u}^T) \mathbf{W}_{m_s}^\theta] \left[ \prod_{j=1}^{s-1} (\mathbf{u}^T \mathbf{W}_{m_j}^\theta \mathbf{u}) \right] \\ &= \sum_{\substack{\{n_1, \dots, n_t\} \in \mathcal{C}(n) \\ \{m_1, \dots, m_s\} \in \mathcal{C}(m)}}} \left[ \prod_{i=1}^{t-1} \left( \frac{1}{N^{n_i}} \mathbf{u}^T \mathbf{W}_{n_i}^\theta \mathbf{u} \right) \right] \left[ \frac{1}{N^{n_t+m_s}} \mathbf{u}^T \mathbf{W}_{n_t}^\theta (\boldsymbol{\Theta} + \mathbf{u} \mathbf{u}^T) \mathbf{W}_{m_s}^\theta \mathbf{u} \right] \\ &\quad \times \left[ \prod_{j=1}^{s-1} \left( \frac{1}{N^{m_j}} \mathbf{u}^T \mathbf{W}_{m_j}^\theta \mathbf{u} \right) \right]. \end{aligned} \quad (\text{A6})$$

If  $t = 1$ , we define the product  $[\prod_{i=1}^{t-1} (\mathbf{W}_{n_i}^\theta \mathbf{H})] = \mathbf{I}$ .

We now prove Eq. (A3) by induction, assuming Eq. (A2) holds. First, when  $n = m = 1$ , the only compositions are trivial (i.e.,  $\pi_1 = \pi_2 = \{1\}$ ). Equating in this case the right-hand sides of Eq. (7) of the main text and Eq. (A6) gives

$$\kappa_{1,1} + (\kappa_1)^2 = \frac{1}{N^2} \mathbf{u}^T \mathbf{W}_1^\theta \boldsymbol{\Theta} \mathbf{W}_1^\theta \mathbf{u} + \left( \frac{1}{N} \mathbf{u}^T \mathbf{W}_1^\theta \mathbf{u} \right)^2.$$

Since Eq. (A2) for  $n = 1$  gives

$$\kappa_1 = \frac{1}{N} \mathbf{u}^T \mathbf{W}_1^\theta \mathbf{u},$$

we have that Eq. (A3) holds for  $n = m = 1$ . Next, assume Eq. (A3) is true for all  $(p, q)$  such that  $p \leq n$  and  $q < m$ , or  $p < n$  and  $q \leq m$ . That is, in these cases,

$$\kappa_p = \frac{1}{N^p} \mathbf{u}^T \mathbf{W}_p^\theta \mathbf{u} \text{ [by Eq. (A2)] and}$$

$$\kappa_{p,q} = \frac{1}{N^{p+q}} \mathbf{u}^T \mathbf{W}_p^\theta \boldsymbol{\Theta} \mathbf{W}_q^\theta \mathbf{u}.$$

Making the corresponding substitutions in Eq. (A6), the only terms we have not accounted for in matching the right-hand side of Eq. (A6) to that of Eq. (7) of the main text are the terms corresponding to the pair of compositions  $\{n\}, \{m\}$ .

In Eq. (7) of the main text, the corresponding terms are

$$\kappa_{n,m} + \kappa_n \kappa_m, \quad (\text{A7})$$

while in Eq. (A6), the terms take the form

$$\begin{aligned} &\frac{1}{N^{n+m}} \mathbf{u}^T \mathbf{W}_n^\theta (\boldsymbol{\Theta} + \mathbf{u} \mathbf{u}^T) \mathbf{W}_m^\theta \mathbf{u} \\ &= \frac{1}{N^{n+m}} \mathbf{u}^T \mathbf{W}_n^\theta \boldsymbol{\Theta} \mathbf{W}_m^\theta \mathbf{u} + \left( \frac{1}{N^n} \mathbf{u}^T \mathbf{W}_n^\theta \mathbf{u} \right) \left( \frac{1}{N^m} \mathbf{u}^T \mathbf{W}_m^\theta \mathbf{u} \right) \\ &= \frac{1}{N^{n+m}} \mathbf{u}^T \mathbf{W}_n^\theta \boldsymbol{\Theta} \mathbf{W}_m^\theta \mathbf{u} + \kappa_n \kappa_m, \end{aligned} \quad (\text{A8})$$

where the second equality follows from the inductive assumption. Comparing Eqs. (A7) and (A8) gives

$$\kappa_{n,m} = \frac{1}{N^{n+m}} \mathbf{u}^T \mathbf{W}_n^\theta \boldsymbol{\Theta} \mathbf{W}_m^\theta \mathbf{u},$$

which is exactly Eq. (A3), completing the inductive proof.

## 5. Proof of the theorem on multibranch motifs

*Proof of Theorem 2.* First, we rewrite the left-hand side (LHS) of Eq. (19) to explicitly account for cases with different  $n_j$  nonzero. Specifically, we sum over all possible sets of  $k \leq k'$  indices  $\{j_1, \dots, j_k\}$  corresponding to the nonzero values of

$n_j$ :

$$\sum_{n_1, \dots, n_{k'}=0}^{\infty} \mu_{n_1, \dots, n_{k'}} = \sum_{\substack{\{j_1, \dots, j_k\} \\ \subset \{1, \dots, k'\}}} \sum_{n_{j_1}, \dots, n_{j_k}=1}^{\infty} \mu_{n_{j_1}, \dots, n_{j_k}}. \quad (\text{A9})$$

We now focus on a fixed  $k$ , and without loss of generality, let  $\{j_1, \dots, j_k\} = \{1, \dots, k\}$ . Applying Eq. (18), we have

$$\begin{aligned} &\sum_{n_1, \dots, n_k=1}^{\infty} \mu_{n_1, \dots, n_k} \\ &= \sum_{n_1, \dots, n_k=1}^{\infty} \sum_{\pi_1, \dots, \pi_k} \left( \prod_{i=1}^k \prod_{j=2}^{t_i} \kappa_{B_j^i} \right) \left( \sum_{\chi} \prod_{\{i_1, \dots, i_s\} \in \chi} \kappa_{B_1^{i_1}, \dots, B_1^{i_s}} \right) \\ &= \sum_{\chi} \sum_{B_1^{i_1}, \dots, B_1^{i_s} \geq 1} \prod_{\{i_1, \dots, i_s\} \in \chi} \kappa_{B_1^{i_1}, \dots, B_1^{i_s}} \\ &\quad \times \left[ \sum_{n_1, \dots, n_k} \sum_{\pi_1, \dots, \pi_k} \left( \prod_{i=1}^k \prod_{j=2}^{t_i} \kappa_{B_j^i} \right) \right]. \end{aligned}$$

In the last equality, we switched the order of summations by pulling the sum over  $\chi$  to the front. Consequently, for each fixed  $\{B_1^{i_1}, \dots, B_1^{i_s}\}$  taken in an outer sum, the  $\{\pi_i\}$  and  $\{n_i\}$  are restricted to terms that are possible for that  $\{B_1^{i_1}, \dots, B_1^{i_s}\}$ . Notice that these sums can be factorized as

$$\sum_{n_1, \dots, n_k} \sum_{\pi_1, \dots, \pi_k} \left( \prod_{i=1}^k \prod_{j=2}^{t_i} \kappa_{B_j^i} \right) = \prod_{i=1}^k \left( \sum_{n_i \geq B_1^{i_1}} \sum_{\pi_i \ni B_1^i} \prod_{j=2}^{t_i} \kappa_{B_j^i} \right). \quad (\text{A10})$$

We next simplify the factors on the right-hand side (RHS) of Eq. (A10). First, we shift the (dummy) indices of summation and multiplication to explicitly begin counting at the second block in the branch:

$$\sum_{n_i \geq B_1^i} \sum_{\pi_i \ni B_1^i} \prod_{j=2}^{t_i} \kappa_{B_j^i} = \sum_{n'_i=0}^{\infty} \sum_{\pi'_i} \prod_{j=1}^{t'_i} \kappa_{B_{j+1}^i},$$

where  $n'_i = n_i - B_1^i$ ,  $\pi'_i = \pi_i \setminus \{B_1^i\}$  and  $t'_i = t_i - 1$  as we exclude the  $B_1^i$  component. For simplicity, we will drop the primes in the summation indices, and then let  $B_j^i$  range over the components of the resulting partition (thus rewriting  $j + 1 \rightarrow j$  below). Doing this, and further rearranging the terms, we have

$$\begin{aligned} \sum_{n_i=0}^{\infty} \sum_{\pi_i} \prod_{j=1}^{t_i} \kappa_{B_j^i} &= \sum_{t_i=0}^{\infty} \sum_{n_i \geq t_i} \sum_{\pi_i} \prod_{j=1}^{t_i} \kappa_{B_j^i} = \sum_{t_i=0}^{\infty} \prod_{j=1}^{t_i} \sum_{B_j^i=1}^{\infty} \kappa_{B_j^i} \\ &= \sum_{t_i=0}^{\infty} \left( \sum_{n_i=1}^{\infty} \kappa_{n_i} \right)^{t_i} = \left( 1 - \sum_{n=1}^{\infty} \kappa_n \right)^{-1}, \end{aligned}$$

where we have summed the geometric series in the last inequality (note the convergence criterion in the Theorem statement).

Therefore, Eq. (A10) and the expression above it yield

$$\begin{aligned} &\sum_{n_1, \dots, n_k=1}^{\infty} \mu_{n_1, \dots, n_k} \\ &= \sum_{\chi} \sum_{B_1^{i_1}, \dots, B_1^{i_s} \geq 1} \prod_{\{i_1, \dots, i_s\} \in \chi} \kappa_{B_1^{i_1}, \dots, B_1^{i_s}} \left( 1 - \sum_{n=1}^{\infty} \kappa_n \right)^{-k} \\ &= \left( 1 - \sum_{n=1}^{\infty} \kappa_n \right)^{-k} \sum_{\chi} \prod_{\{i_1, \dots, i_s\} \in \chi} \left( \sum_{B_1^{i_1}, \dots, B_1^{i_s} \geq 1} \kappa_{B_1^{i_1}, \dots, B_1^{i_s}} \right) \\ &= (1 - q)^{-k} \sum_{\chi} \prod_{\{i_1, \dots, i_s\} \in \chi} \left( \sum_{B_1^{i_1}, \dots, B_1^{i_s} \geq 1} \kappa_{B_1^{i_1}, \dots, B_1^{i_s}} \right), \end{aligned}$$

where we let  $q = \sum_{n=1}^{\infty} \kappa_n$ . The above gives a useful expression for the sum over all motifs with exactly  $k$  branches of nonzero length. To establish the theorem, we use this expression for different subsets of  $\{1, \dots, k'\}$  (hence different  $k$ ) that occur in Eq. (A9). Doing this, we have

$$\begin{aligned} \sum_{n_1, \dots, n_{k'}=0}^{\infty} \mu_{n_1, \dots, n_{k'}} &= \sum_{\substack{\{j_1, \dots, j_k\} \\ \subset \{1, \dots, k'\}}} \sum_{\chi_k} (1 - q)^{-k} \\ &\quad \times \prod_{\{i_1, \dots, i_s\} \in \chi_k} \left( \sum_{B_1^{i_1}, \dots, B_1^{i_s} \geq 1} \kappa_{B_1^{i_1}, \dots, B_1^{i_s}} \right), \end{aligned}$$

where  $\chi_k$  is a partition of the set  $\{j_1, \dots, j_k\}$  (though we only use the subscript  $k$ ,  $\chi_k$  should actually depend on the set  $\{j_1, \dots, j_k\}$ ). We next rearrange this expression. First, we define a lift of each partition  $\chi_k$  to a partition  $\chi$  of the set  $\{1, \dots, k'\}$ , by adding any indices not present in  $\chi_k$  as individual groups  $\{i_{k+1}\}, \dots, \{i_{k'}\}$ . Next we split the sum across  $\{j_1, \dots, j_k\}$  and  $\chi_k$  according to their resulting lift  $\chi$ . This creates an outer sum; here, the range of  $\chi$  is all possible partitions of  $\{1, \dots, k'\}$ . Thus, the expression above is

$$= \sum_{\chi} \sum_{\chi_k \setminus \chi} (1 - q)^{-k} \prod_{\{i_1, \dots, i_s\} \in \chi_k} \left( \sum_{B_1^{i_1}, \dots, B_1^{i_s} \geq 1} \kappa_{B_1^{i_1}, \dots, B_1^{i_s}} \right).$$

The inner sum is over all  $\chi_k$ ,  $0 \leq k \leq k'$  whose lift is  $\chi$ . We can pull out all factors associated with groups in  $\chi_k$  that have only 1 element. Note that each of such group  $\{i_r\}$  corresponds to a factor  $\sum_{B_1^{i_r} \geq 1} \kappa_{B_1^{i_r}} = q$ . Therefore, the rest of the factors in  $\prod_{\{i_1, \dots, i_s\} \in \chi_k} \kappa_{B_1^{i_1}, \dots, B_1^{i_s}}$  are  $(k - m_2) q$ -factors, where  $m_2$  is the number of indices that are partitioned into a group with more than one

element in  $\chi_k$  (or  $\chi$ ). Thus, the expression above is

$$\begin{aligned}
 &= \sum_{\chi} \sum_{\chi_k | \chi} (1-q)^{-k} q^{k-m_2} \\
 &\quad \times \prod_{\substack{\{i_1, \dots, i_s\} \in \chi_k, \\ s > 1}} \left( \sum_{B_1^{i_1}, \dots, B_1^{i_s} \geq 1}^{\infty} \kappa_{B_1^{i_1}, \dots, B_1^{i_s}} \right) \\
 &= (1-q)^{-k'} \sum_{\chi} \prod_{\substack{\{i_1, \dots, i_s\} \in \chi, \\ s > 1}} \left( \sum_{B_1^{i_1}, \dots, B_1^{i_s} \geq 1}^{\infty} \kappa_{B_1^{i_1}, \dots, B_1^{i_s}} \right) \\
 &\quad \times \left( \sum_{\chi_k | \chi} q^{k-m_2} (1-q)^{k'-k} \right).
 \end{aligned}$$

For a fixed  $k$ , it is easy to see the number of  $\chi_k$  whose lift being  $\chi$  is  $\binom{k'-m_2}{k-m_2}$ . Hence,

$$\sum_{\chi_k | \chi} q^{k-m_2} (1-q)^{k'-k} = \sum_{k=0}^{k'} \binom{k'-m_2}{k-m_2} q^{k-m_2} (1-q)^{k'-k} = 1.$$

Finally, the expression above is

$$\begin{aligned}
 &= (1-q)^{-k'} \sum_{\chi} \prod_{\substack{\{i_1, \dots, i_s\} \in \chi, \\ s > 1}} \left( \sum_{B_1^{i_1}, \dots, B_1^{i_s} \geq 1}^{\infty} \kappa_{B_1^{i_1}, \dots, B_1^{i_s}} \right) \\
 &= (1-q)^{-k'} \sum_{\pi} f(\pi) \prod_{B \in \pi, B > 1} \left( \sum_{n_1, \dots, n_B = 1}^{\infty} \kappa_{n_1, \dots, n_B} \right).
 \end{aligned}$$

In the last line, since the factor with  $\kappa_*$  is the same as long as  $s$  is the same, regardless of the actual value of  $i_1, \dots, i_s$ , we switched from summing over set partitions  $\chi$  to corresponding integer partitions  $\pi$  of  $k'$ . This introduces the  $f(\pi)$  factor and finishes the proof [see Eq. (19)].

## 6. Establishing the subpopulation cumulant corollary (12)

Beyond the similarity in appearance between the single population and subpopulation formulas given by Eqs. (8) and (12), these two can be precisely connected. Define a new product between two matrices (or tensors) as

$$(\mathbf{A} \odot \mathbf{B})_{ij} = \sum_k \mathbf{A}_{ik} \mathbf{B}_{jk} \frac{N_k}{N}. \quad (\text{A11})$$

It is easy to see that Eqs. (10) and (11) are equivalent to Eqs. (6) and (7) when the product is interpreted as  $\odot$ . Very much like the ordinary matrix multiplication,  $\odot$  is noncommutative, but is associative and distributive, which are all that we need for the theory. This shows that Eq. (12) can be proved identically as the single population case given by Eq. (8) while interpreting products via  $\odot$ .

## 7. Subpopulation theory for higher-order correlations

The idea in this Appendix, Sec. 6, is exactly how we will develop the subpopulation theory for higher-order correlations.

Under the interpretation of  $\odot$ , the relationship among subpopulation motif moments and cumulants can be written as

$$\mu_{n_1, \dots, n_k} = \sum_{\pi_1, \dots, \pi_k} \left( \bigotimes_{i=1}^k \prod_{j=2}^{t_i} \kappa_{B_j^{i_1}} \right) \left( \sum_{\chi} \bigodot_{\{i_1, \dots, i_s\} \in \chi} \kappa_{B_1^{i_1}, \dots, B_1^{i_s}} \right). \quad (\text{A12})$$

As before,  $\pi_i = \{B_1^{i_1}, \dots, B_{t_i}^{i_1}\}$  is an ordered partition of  $n_i$ . Moreover,  $\chi$  is a partition of the set  $\{1, \dots, k\}$  and  $\{i_1, \dots, i_s\}$  is one set of indices that are grouped together under  $\chi$ . Here,  $\mu_{n_1, \dots, n_k}$  (for  $k \geq 2$ ) is a  $k$ -dimensional tensor: each entry  $\mu_{n_1, \dots, n_k}^{\alpha_1, \dots, \alpha_k}$  represents the frequency of a  $k$ -branch motif with endpoints in subpopulation  $\alpha_1, \dots, \alpha_k$ , respectively. Notably, there is a third type of quantity appearing in Eq. (A12):  $\kappa_{B_1^{i_1}, \dots, B_1^{i_s}, \cdot}$ , which is a  $s+1$  tensor ( $s \geq 2$ ). The extra dimension (represented by the dot in the subscript) comes from specifying the subpopulation of the root node, beside the subpopulation of the endpoints. This is the same situation as for one-branch or chain motifs  $\mu_{n_1}$  and  $\kappa_{B_1^i}$ , which are 2-tensors ( $b \times b$  matrices) and should formally be written as  $\mu_{n_1, \cdot}$  and  $\kappa_{B_1^i, \cdot}$ ; we omit the dot for these chains as long as it is clear from the context. The big  $\odot$  product forms a  $k$  tensor out of  $|\chi|$  factors, in a way similar to a multivariate trace:

$$\left( \bigodot_{\{i_1, \dots, i_s\} \in \chi} \kappa_{B_1^{i_1}, \dots, B_1^{i_s}, \cdot} \right)^{\alpha_1, \dots, \alpha_k} = \sum_{\beta=1}^b \frac{N_{\beta}}{N} \prod_{\{i_1, \dots, i_s\} \in \chi} \kappa_{B_1^{i_1}, \dots, B_1^{i_s}, \beta}^{\alpha_1, \dots, \alpha_s, \beta}. \quad (\text{A13})$$

As an example, if  $\chi$  only contains one partition, that consists of the set itself, we define  $\kappa_{B_1^{i_1}, \dots, B_1^{i_s}} := \bigodot \kappa_{B_1^{i_1}, \dots, B_1^{i_s}, \cdot}$ . It is not hard to see that the meaning of the resulting  $s$ -tensor  $\kappa_{B_1^{i_1}, \dots, B_1^{i_s}}^{\alpha_1, \dots, \alpha_s}$  is the motif cumulant with specified subpopulations for the endpoints.

The tensor product “ $\bigotimes_{j=1}^k$ ” in Eq. (A12) is simply a weighted version of the ordinary tensor product, that is,

$$\left( \bigotimes_{j=1}^k \mathbf{P}_j \cdot \mathbf{A} \right)^{\alpha_1, \dots, \alpha_k} = \sum_{\beta_1, \dots, \beta_k} \left( \prod_{j=1}^k \frac{N_j}{N} (\mathbf{P}_j)_{\alpha_j, \beta_j} \right) \mathbf{A}^{\beta_1, \dots, \beta_k}. \quad (\text{A14})$$

Despite the difference in notation between Eqs. (A12) and (18), the operations share some basic algebraic properties, namely, being associative and distributive—which are all that is needed in the proof of Eq. (21). This allows us to derive, with identical arguments, the subpopulation result:

*Corollary 2.*

$$\begin{aligned}
 \frac{\langle \mathbf{S}_{y[k]} \rangle_B}{S_{x[k]}} &= \frac{1}{N^{k-1}} \bigotimes_{i=1}^k \left( \mathbf{I} - \sum_{n=1}^{\infty} g^n \kappa_n \right)^{-1} \\
 &\quad \times \left[ \sum_{\chi} \bigodot_{\{i_1\} \in \chi} \mathbf{E}^{-1} \bigodot_{\{i_1, \dots, i_s\} \in \chi, s > 1} \right. \\
 &\quad \left. \times \left( \sum_{n_1, \dots, n_s=1}^{\infty} g^{|n|} \kappa_{n_1, \dots, n_s, \cdot} \right) \right]. \quad (\text{A15})
 \end{aligned}$$

Here, the two “ $\odot$ ” terms are actually two parts of one single product associated with  $\chi$ , as defined in Eq. (A13). Specifically,

$$\left[ \odot_{\{i_1\} \in \chi} \mathbf{E}^{-1} \odot_{\{i_1, \dots, i_s\} \in \chi, s > 1} \left( \sum_{n_1, \dots, n_s=1}^{\infty} g^{|n|} \kappa_{n_1, \dots, n_s} \right) \right]^{\alpha_1, \dots, \alpha_k} = \sum_{\beta=1}^b \frac{N_\beta}{N} \prod_{\{i_1\} \in \chi} (\mathbf{E}^{-1})_{\alpha_{i_1} \beta} \prod_{\{i_1, \dots, i_s\} \in \chi} \kappa_{B_1^{i_1}, \dots, B_1^{i_s}}^{\alpha_{i_1}, \dots, \alpha_{i_s}, \beta}.$$

We emphasize again that all multiplicative operations in the formula above should be interpreted as for  $\odot$ .

However, it is also easy to rewrite this expression using only ordinary products, by inserting the diagonal scaling matrix  $\mathbf{E}$ . For example, enumerating the terms for third-order correlation ( $k = 3$ ) yields

$$\begin{aligned} \langle \mathbf{S}_{y[3]} \rangle_B / S_{x[3]} &= \frac{1}{N^2} \left( \mathbf{I} - \sum_{l=1}^{\infty} g^l \kappa_l \mathbf{E} \right)^{-1} \otimes \left( \mathbf{I} - \sum_{m=1}^{\infty} g^m \kappa_m \mathbf{E} \right)^{-1} \otimes \left( \mathbf{I} - \sum_{n=1}^{\infty} g^n \kappa_n \mathbf{E} \right)^{-1} \\ &\times \left[ \mathbf{E}_{[3]}^{-2} + \sum_{l,m=1}^{\infty} g^{l+m} (\kappa_{l,m,\cdot} + \kappa_{l,\cdot,m} + \kappa_{\cdot,l,m}) + \sum_{l,m,n=1}^{\infty} g^{l+m+n} \kappa_{l,m,n} \right]. \end{aligned} \quad (\text{A16})$$

Here,  $\mathbf{E}_{[3]}^{-2}$  is a diagonal 3-tensor, with  $(\mathbf{E}_{[3]}^{-2})^{\alpha\beta\gamma} = \delta_{\alpha\beta\gamma} (\frac{N_\alpha}{N})^{-2}$ .  $\kappa_{l,\cdot,m}$  and  $\kappa_{\cdot,l,m}$  are transpositions of the tensor  $\kappa_{l,m,\cdot}$ , i.e.,  $(\kappa_{l,m,\cdot})^{i_1, i_2, i_3} = (\kappa_{l,\cdot,m})^{i_1, i_3, i_2} = (\kappa_{\cdot,l,m})^{i_3, i_1, i_2}$ .

- 
- [1] P. Bonifazi *et al.*, *Science* **326**, 1419 (2009).
- [2] S. Song, P. J. Sjöström, M. Reigl, S. Nelson, and D. B. Chklovskii, *PLoS Biol.* **3**, e68 (2005).
- [3] R. Perin, T. K. Berger, and H. Markram, *Proc. Natl. Acad. Sci. USA* **108**, 5419 (2011).
- [4] R. Milo *et al.*, *Science* **303**, 1538 (2004).
- [5] P. Larimer and B. W. Strowbridge, *J. Neurosci.* **28**, 12212 (2008).
- [6] L. M. Pecora and T. L. Carroll, *Phys. Rev. Lett.* **80**, 2109 (1998).
- [7] S. Strogatz, *Physica D* **143**, 1 (2000).
- [8] J. Rinzel and G. B. Ermentrout, in *Methods in Neuronal Modeling*, edited by C. Koch and I. Segev (MIT Press, Cambridge, MA, 1989), pp. 135–169.
- [9] We quantify second-order correlations between the activity of two nodes  $i, j$  using the cross-covariance functions, defined by  $(C_y(\tau))_{ij} = \mathbf{E}(\{y_i(t) - \mathbf{E}[y_i(t)]\} \{y_j(t + \tau) - \mathbf{E}[y_j(t + \tau)]\})$ .
- [10] A. Renart *et al.*, *Science* **327**, 587 (2010).
- [11] V. Pernice, B. Staude, S. Cardanobile, and S. Rotter, *PLoS Comput. Biol.* **7**, e1002059 (2011).
- [12] V. Pernice, B. Staude, S. Cardanobile, and S. Rotter, *Phys. Rev. E* **85**, 031916 (2012).
- [13] B. Lindner, B. Doiron, and A. Longtin, *Phys. Rev. E* **72**, 061919 (2005).
- [14] E. Schneidman, S. Still, M. J. Berry, II, and W. Bialek, *Phys. Rev. Lett.* **91**, 238701 (2003).
- [15] P. Fries, *Trends Cogn. Sci.* **9**, 474 (2005).
- [16] W. Singer and C. M. Gray, *Annu. Rev. Neurosci.* **18**, 555 (1995).
- [17] E. Salinas and T. J. Sejnowski, *J. Neurosci.* **20**, 6193 (2000).
- [18] M. Diesmann, M.-O. Gewaltig, and A. Aertsen, *Nature (London)* **402**, 529 (1999).
- [19] A. Pikovsky, M. Rosenblum, and J. Kurths, *Synchronization: A Universal Concept in Nonlinear Sciences* (Cambridge University Press, Cambridge, 2001).
- [20] B. B. Averbeck, P. E. Latham, and A. Pouget, *Nat. Rev. Neurosci.* **7**, 358 (2006).
- [21] T. Gawne and B. Richmond, *J. Neurosci.* **13**, 2758 (1993).
- [22] M. R. Cohen and A. Kohn, *Nat. Neurosci.* **14**, 811 (2011).
- [23] E. Zohary, M. N. Shadlen, and W. T. Newsome, *Nature (London)* **370**, 140 (1994).
- [24] H. Sompolinsky, H. Yoon, K. Kang, and M. Shamir, *Phys. Rev. E* **64**, 051904 (2001).
- [25] L. F. Abbott and P. Dayan, *Neural Comput.* **11**, 91 (1999).
- [26] I. Ginzburg and H. Sompolinsky, *Phys. Rev. E* **50**, 3171 (1994).
- [27] T. Sejnowski, *Biol. Cybern.* **22**, 203 (1976).
- [28] J. Trousdale, Y. Hu, E. Shea-Brown, and K. Josić, *PLoS Comput. Biol.* **8**, e1002408 (2012).
- [29] Y. Hu, J. Trousdale, K. Josić, and E. Shea-Brown, *J. Stat. Mech.* (2013) P03012.
- [30] C. W. Gardiner, *Handbook of Stochastic Methods for Physics, Chemistry and the Natural Sciences* (Springer-Verlag, Berlin, 2009).
- [31] A. G. Hawkes, *J. R. Stat. Soc. Ser. B* **33**, 438 (1971).
- [32] J. M. Pedraza and A. van Oudenaarden, *Science* **307**, 1965 (2005).
- [33] R. Tomioka, H. Kimura, T. J. Kobayashi, and K. Aihara, *J. Theor. Biol.* **229**, 501 (2004).
- [34] I. Lestas, J. Paulsson, N. E. Ross, and G. Vinnicombe, *IEEE Trans. Automat. Contr.* **53**, 189 (2008).
- [35] P. B. Warren, S. Tanase-Nicola, and P. R. Wolde, *arXiv:q-bio/0512041*.
- [36] Spectral quantities of stochastic processes are technically defined by considering first the transform over a finite window, i.e.,  $\tilde{y}(\omega) = \int_0^T dt e^{-2\pi i \omega t} \{y_i(t) - \mathbf{E}[y_i(t)]\}$ . The spectrum, for instance, is given by  $S_y(\omega) = \lim_{T \rightarrow \infty} \frac{1}{T} \mathbf{E}[\tilde{y} \tilde{y}^*(\omega)]$ .
- [37] C. Laing and G. J. Lord, *Stochastic Methods in Neuroscience* (Oxford University Press, Oxford, 2009).
- [38] Y. J. Wang and G. Y. Wong, *J. Am. Stat. Assoc.* **82**, 8 (1987).
- [39] J. J. Daudin, F. Picard, and S. Robin, *Stat. Comput.* **18**, 173 (2008).
- [40] A. Litwin-Kumar and B. Doiron, *Nat. Neurosci.* **15**, 1498 (2012).
- [41] B. J. Pettejohn, M. J. Berryman, and M. D. McDonnell, *Front. Comput. Neurosci.* **5**, 11 (2011).

- [42] R. A. Horn and C. R. Johnson, *Matrix Analysis* (Cambridge University Press, Cambridge, 1990).
- [43] K. Rajan and L. F. Abbott, *Phys. Rev. Lett.* **97**, 188104 (2006).
- [44] D. R. Brillinger, *An Introduction to Polyspectra*, 1964 (unpublished).
- [45] Y. C. Kim and E. Powers, *IEEE Transactions on Plasma Sciences* **7**, 120 (1979).
- [46] P. Huber, B. Kleiner, T. Gasser, and G. Dumermuth, *IEEE Transactions on Audio and Electroacoustics* **19**, 78 (1971).
- [47] U. Alon, *Nat. Rev. Genetics* **8**, 450 (2007).
- [48] J.-P. Pfister and W. Gerstner, *J. Neurosci.* **26**, 9673 (2006).
- [49] J. Zylberberg and E. Shea-Brown, [arXiv:1212.3549](https://arxiv.org/abs/1212.3549).
- [50] Y. Hu, J. Zylberberg, and E. Shea-Brown, *PLoS Comput. Biol.* **10**, e1003469 (2014).